VU VRIJE UNIVERSITEIT AMSTERDAM

VU Research Portal

A computational study of the robustness of cellular oscillators

Paijmans, J.J.

2017

document version
Publisher's PDF, also known as Version of record

Link to publication in VU Research Portal

citation for published version (APA)
Paijmans, J. J. (2017). *A computational study of the robustness of cellular oscillators*. [PhD-Thesis - Research and graduation internal, Vrije Universiteit Amsterdam].

General rights
Copyright and moral rights for the publications made accessible in the public portal are retained by the authors and/or other copyright owners and it is a condition of accessing publications that users recognise and abide by the legal requirements associated with these rights.

- Users may download and print one copy of any publication from the public portal for the purpose of private study or research.
- You may not further distribute the material or use it for any profit-making activity or commercial gain
- You may freely distribute the URL identifying the publication in the public portal ?

Take down policy
If you believe that this document breaches copyright please contact us providing details, and we will remove access to the work immediately and investigate your claim.

E-mail address:
vuresearchportal.ub@vu.nl

Download date: 04. May. 2023

2

DISCRETE GENE REPLICATION EVENTS DRIVE COUPLING BETWEEN THE CELL CYCLE AND CIRCADIAN CLOCKS

Many organisms possess both a cell cycle to control DNA replication and a circadian clock to anticipate changes between day and night. In some cases, these two rhythmic systems are known to be coupled by specific, cross-regulatory interactions. Here, we use mathematical modeling to show that, additionally, the cell cycle generically influences circadian clocks in a non-specific fashion: The regular, discrete jumps in gene-copy number arising from DNA replication during the cell cycle cause a periodic driving of the circadian clock, which can dramatically alter its behavior and impair its function. A clock built on negative transcriptional feedback either phase locks to the cell cycle, so that the clock period tracks the cell division time, or exhibits erratic behavior. We argue that the cyanobacterium Synechococcus elongatus *has evolved two features that protect its clock from such disturbances, both of which are needed to fully insulate it from the cell cycle and give it its observed robustness: a phosphorylation-based protein modification oscillator, together with its accompanying push-pull read-out circuit that responds primarily to the ratios of the different phosphoforms, makes the clock less susceptible to perturbations in protein synthesis; and the presence of multiple, asynchronously replicating copies of the same chromosome diminishes the effect of replicating any single copy of a gene.*

The content of this chapter has been published as Joris Paijmans, Mark Bosman, Pieter Rein ten Wolde, and David K. Lubensky. *Discrete gene replication events drive coupling between the cell cycle and circadian clocks.* Proc Natl Acad Sci **113**, 22:4063–4068, 2016 [21].

2.1. INTRODUCTION

Circadian clocks—autonomous oscillators with a roughly 24 hour period that can be entrained to daily cycles of light and dark —are thought to confer important advantages on living cells by allowing them to anticipate diurnal environmental changes. Recent decades have seen considerable progress in elucidating both the architecture and the function of these biological timekeepers. Circadian clocks, however, are not the only oscillatory systems present in living cells. Most notably, cell growth and division are governed by a cell cycle, which can in many contexts be viewed as an autonomous oscillator. Much recent attention has been directed towards the connections between these two rhythmic systems, which are relevant for processes ranging from plants' response to shade [31] to cancer susceptibility [32, 33]. In particular, it is now clear that circadian clocks can exert specific regulatory influences on the cell cycle, and a number of experimental and modeling studies have sought to tease out the implications of this regulation [3, 34–40]. Here, we argue that, in addition to direct, specific regulation of one oscillator by the other, there must also be more generic connections between the circadian clock and the cell cycle [32, 39–41]. In particular, we focus on the consequences of the discrete gene replication events that accompany DNA replication. We show that, as a result of the regular jumps in gene copy number caused by these events, the cell cycle must, very generally, contribute a periodic forcing to the circadian clock. This forcing can markedly change clock behavior and degrade clock function. We propose that cyanobacterial clocks have evolved specific features that can mitigate this effect. More broadly, this generically strong coupling to the cell cycle implies important constraints on the design of biological timekeepers if they are to remain accurate in dividing cells.

It is widely accepted that protein levels depend on a cell's gene dosage. As was recently shown experimetnally, a doubling of the number of chromosomal copies of a gene results in an approximate doubling of its mRNA synthesis rate and thus to a corresponding increase in its protein levels [4]. Most often, however, such effects are considered in the context of a change in the number of autosomal gene copies that persists throughout an organism's lifetime [42], as, e.g., in the haploinsufficiency of certain genes [43]. It is less often acknowledged that the number of copies of all genes varies over each cell cycle, despite evidence that these variations have measurable consequences [4, 44–47]. Because of the well-known phenomenon of phase locking of oscillators [48], regular, periodic changes in gene dose are likely to be especially relevant to cellular oscillators that depend on gene expression. A circadian clock that became slaved to the cell cycle, for example, would lose its identity as an autonomous timekeeper, and thus much of its ability to perform its biological function. Here, we show that oscillators built on negative transcriptional feedback—a common motif in both prokaryotic and eukaryotic clocks—are indeed very strongly affected by driving from periodic gene replication events. This immediately raises the question of how real biological clocks are able to function in growing, dividing cells. To address this, we study the circadian clock of the cyanobacterium *Synechococcus elongatus*, which is known to exhibit stable rhythms over a wide range of growth rates [20, 49], but whose clock appears not to regulate DNA replication [3], suggesting exactly the sort of unidirectional forcing of the clock by the cell cycle that might have been expected to impair clock function.

The *S. elongatus* clock combines a negative transcriptional feedback oscillator (the

transcription-translation cycle, or TTC) with a core phosphorylation-based post-translational oscillator (the protein phosphorylation cycle, or PPC). This clock is known to comprise two parts, a phosphorylation-based post-translational oscillator (the protein phosphorylation cycle, or PPC) whose core consists of the proteins KaiA, KaiB, and KaiC, and a more conventional module based on negative transcriptional feedback (the transcription-translation cycle, or TTC). Remarkably, the PPC can be reconstituted *in vitro* with purified proteins [12], allowing detailed study of the mechanisms behind its oscillation. A number of studies have begun to converge on the view that the PPC works by synchronizing the intrinsic phosphorylation cycles of individual KaiC hexamers, primarily through phosphorylation-dependent sequestration of KaiA by KaiC [15, 18, 22, 50–53]. Although many details of the TTC remain murkier, it seems clear that the protein RpaA plays a central role, regulating the expression of clock components in a manner that ultimately reflects the KaiC phosphorylation state [27, 54–57]. Depending on light and nutrient levels, *S. elongatus* can have doubling times ranging from 6 to 72 h [20]; the cell cycle period is thus of the same order as the clock period of roughly 24 h, opening the way for interactions between the two. Indeed, the circadian clock is known to gate mitosis, prohibiting cell division during certain clock phases [3, 36, 37], although in constant light this gating leaves both DNA replication and cell growth essentially unchanged [3]. Conversely, Mori and Johnson argued that cell growth and division don't affect the *S. elongatus* circadian clock [49]. We use mathematical modeling to study the unidirectional forcing of the clock by the cell cycle. We identify specific features of the *S. elongatus* clock that tend to insulate it from entrainment by regular gene replication events. Nonetheless, we argue that, under certain conditions, it should be possible to observe signatures of periodic forcing of the clock by the cell cycle. We further suggest how some of the clock's protective mechanisms might be weakened experimentally, leading to much stronger signatures of its coupling to the cell cycle.

Below, we first model the effects of cell growth and division on a constitutively expressed protein. We show that gene replication, not cell division, is the essential cell-cycle event that influences protein concentrations and that, as long as the constitutively expressed protein is not subject to rapid, active degradation, its concentration varies little over the cell cycle. In contrast, gene replication —which introduces a periodic forcing that drives the circadian clock— can dramatically affect the behavior of a negative transcriptional feedback oscillator (NTFO): the NTFO locks to the cell cycle over a range of cell-division times of many hours and shows erratic behavior outside this regime [41]. Such an oscillator cannot function as a clock. We next ask how the real cyanobacterial clock can be so apparently undisturbed by the cell cycle. We find that incorporating both a PPC and a TTC into the clock significantly weakens coupling to the cell cycle, especially when the clock is read out by a push-pull network that is more sensitive to ratio of concentrations of different phosphorylation states than to their absolute values. The presence of multiple chromosome copies has a still more striking effect: If the cell has 4 copies after division (rather than only 1), as can often be the case in *S. elongatus*, and if these are replicated one after the other [58], then the dose of the clock genes changes much more gradually, and cell cycle effects are almost completely lost. Thus, *S. elongatus* may have evolved to carry multiple, identical chromosome copies in part to insulate its circadian clock from its DNA replication cycles.

2.2. MODELS AND RESULTS

2.2.1. THE CELL CYCLE'S EFFECT ON A CONSTITUTIVELY EXPRESSED GENE IS WEAK

Before turning to the more complex case of a circadian clock, we first investigate how the concentration of a single, constitutively expressed protein varies over a cell cycle [4]. To this end, we add regular, rhythmic DNA replication and mitosis to a simple model of protein production and dilution.

The key quantities in our description are the number of copies $g(t)$ of the gene of interest and the cell volume $V(t)$. These vary periodically in time as sketched in Fig. 2.1A–B, with a period given by the cell division time T_d. We assume for now that there is only one gene copy present immediately after cell division. This copy is replicated at some time before the next division, at which point $g(t)$ jumps from 1 to 2. When the cell divides, the chromosomes are split between the daughter cells, and $g(t)$ returns to 1. The cell volume grows exponentially: $V(t) = V_0 \exp(\mu_\mathrm{d} t)$, with $\mu_\mathrm{d} = \log(2)/T_\mathrm{d}$. When t reaches T_d, division occurs, and $V(t)$ drops back from $2V_0$ to V_0.

The variables $g(t)$ and $V(t)$ define the gene density $G(t) \equiv g(t)/V(t)$. As long as noise and spatial variations are neglected, the behavior of a biochemical network depends only on protein *concentrations*, not separately on protein numbers and cell volume. As a result, the system responds to the protein synthesis rate per unit volume, proportional to $G(t)$, but not to $g(t)$ and $V(t)$ individually (Eq. 2.1, below). Fig. 2.1C shows that $G(t)$ has only a single discontinuity during the cell cycle, corresponding to the doubling of $g(t)$ when the gene is copied; at cell division, both $g(t)$ and $V(t)$ are halved, so their ratio is unchanged. Importantly, then, the meanfield, deterministic dynamics of a biochemical network is sensitive to the timing of DNA replication but not of cell division. This dynamics is likewise unaffected by any gating of cell division by the circadian clock, provided, as is the case in *S. elongatus* [3, 37], that this gating does not affect DNA replication or cell growth. Similarly, regardless of when during the division cycle the gene is copied, the time dependence of $G(t)$ is always the same: It doubles, decays exponentially for a time T_d, then doubles again, etc. The exact moment of gene replication affects only the average value of $G(t)$, which can be absorbed, for modeling purposes, into the parameter β (Eq. 2.1, below). For simplicity, we thus always assume that the gene is replicated exactly at $t = T_\mathrm{d}/2$.

Given the gene density $G(t)$, the concentration $C(t)$ of a constitutively expressed protein evolves as:

$$\frac{dC(t)}{dt} = \beta G(t) - \mu_\mathrm{d} C(t). \tag{2.1}$$

Here, proteins are expressed at a rate β per gene copy and diluted by cell growth at a rate $\mu_\mathrm{d} = \log(2)/T$. We thus assume that, as is true for many bacterial proteins, the protein is not subject to active degradation [59]. Fig. 2.1D shows how $C(t)$ varies over the cell cycle. Remarkably, even though the protein production rate doubles each time the gene is replicated, the protein concentration varies by no more than a few percent: The discrete jumps in protein production are smoothed out by the slow protein dilution. Thus, a protein that is constitutively expressed and not actively degraded is little affected by the cell cycle.

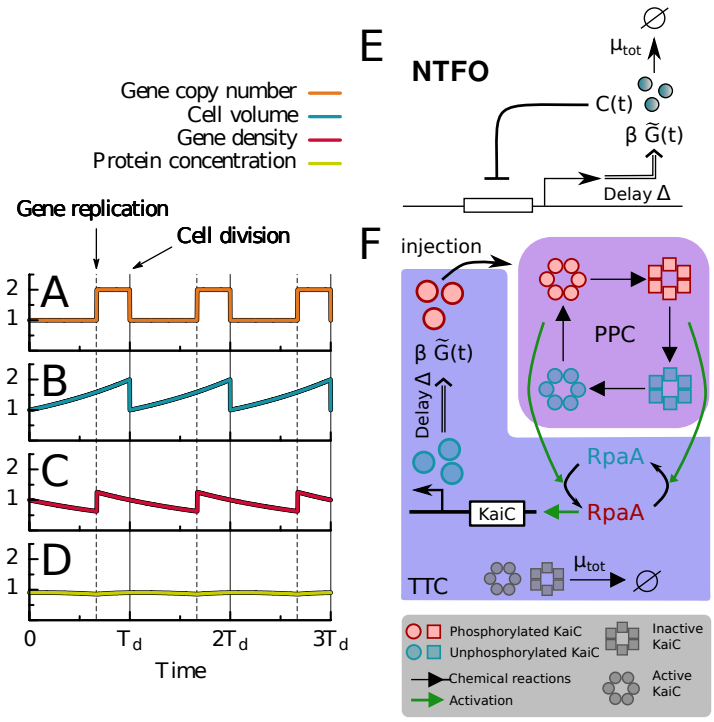

Figure 2.1: DNA replication but not cell division affects average expression levels; for a protein that is constitutively expressed and decays by dilution only, the effect is small. Schematic time courses of the gene copy number $g(t)$ (A), the cell volume $V(t)$ (B), the gene density, $G(t) = g(t)/V(t)$ (C), and the concentration $C(t)$ of a constitutively expressed protein that decays only by dilution (D). Time in units of the cell division time T_d; vertical axes, arbitrary units. The gene density (C) has a discontinuity when the gene is replicated (vertical dotted lines) but not at cell division (vertical solid lines), when both $g(t)$ and $V(t)$ are halved. Even though the protein synthesis rate doubles when the gene is replicated, the maximum deviation of $C(t)$ from its time average is less than 4% (D). (E) The NTFO model: A protein with concentration $C(t)$ represses its own transcription with a delay Δ. (F) Zwicker [19] model for coupled phosphorylation (PPC, purple background) and transcription-translation (TTC, blue background) cycles. KaiC hexamers switch between an active conformational state (circles) in which their phosphorylation level tends to rise and an inactive state (squares) in which it tends to fall. Active KaiC activates RpaA and inactive KaiC inactivates RpaA; active RpaA (red) activates *kaiBC* expression, leading (after a delay) to the injection of fully phosphorylated KaiC (pink) into the PPC.

2.2.2. THE CELL CYCLE STRONGLY PERTURBS BOTH THE PERIOD AND THE AMPLITUDE OF A NEGATIVE TRANSCRIPTIONAL FEEDBACK OSCILLATOR

Although the concentration of a protein that is constitutively expressed does not vary much over the cell cycle, oscillators are known to be far more sensitive to periodic driving

than non-oscillatory systems [48]. We thus next consider a simple model for a clock built on delayed, negative transcriptional feedback (Fig. 2.1E). The model consists of a single variable, $C(t)$, describing the concentration of proteins that inhibit their own production:

$$\frac{dC(t)}{dt} = \beta \tilde{G}(t) \frac{K_c^n}{K_c^n + C(t-\Delta)^n} - \mu_{\text{tot}} C(t). \tag{2.2}$$

We impose a fixed delay Δ between the initiation of transcription and the appearance of functional proteins. Therefore, protein production at time t is proportional to the gene copy number $g(t-\Delta)$ at time $t-\Delta$. These proteins 'arrive' in the cell volume $V(t)$ at time t. The protein synthesis rate per unit volume at time t is thus proportional to the *protein production density* $\tilde{G}(t) \equiv g(t-\Delta)/V(t)$. $\tilde{G}(t)$ is a generalization of the gene density $G(t)$ of the preceding section to the case with a delay Δ and parametrizes the periodic forcing of the NTFO by gene replication. Proteins disappear with a total rate $\mu_{\text{tot}} = \mu_{\text{d}} + \mu_{\text{act}}$, where as before μ_{d} describes dilution due to cell growth, and μ_{act} describes possible active degradation. Including both terms allows us to vary the doubling time T_{d} while holding μ_{tot} constant and hence, in our simulations, to distinguish the trivial influence of the cell cycle on the clock through the dilution rate μ_{d} from other effects.

We next define the peak-to-peak time T_{PtP} as the time between successive peaks in $C(t)$ (see Fig. 2.2 and *Supporting Information* [SI]); T_{PtP} reduces to the period of the circadian clock when oscillations are regular but remains defined when the cell cycle induces more erratic behavior. In Fig. 2.2A we plot the average peak-to-peak time $\langle T_{\text{PtP}} \rangle$ for a range of division times T_{d} at fixed μ_{tot}.

As expected from the general theory of driven oscillators [48], the curve shows two striking features: First, around division times which are fractions or multiples of the clock's intrinsic period of 24 h, the cell cycle determines the period of the clock. Especially around $T_{\text{d}} = 24$ and 48 h, the average peak to peak time is directly proportional to T_{d}. At $T_{\text{d}} = 24$ h (1:1 locking), $\langle T_{\text{PtP}} \rangle = T_{\text{d}}$, and the amplitude of each clock oscillation cycle is the same (Fig. 2.2B). At $T_{\text{d}} = 48$ h (2:1 locking), however, $\langle T_{\text{PtP}} \rangle = T_{\text{d}}/2$, and two full clock cycles are required to make up a single division time. Because these two cycles occur at different gene densities, successive peaks in the trace of $C(t)$ have alternately large and small amplitudes.

Second, the standard deviation of T_{PtP} becomes very large just outside the locking regions. Fig. 2.2C shows that this variability in the phase of $C(t)$ is accompanied by substantial fluctuations in the amplitude for $T_{\text{d}} = 27$ h. Because the difference between T_{d} and the intrinsic clock period is just too large to allow stable locking, the clock constantly tries to lock to the cell cycle, but slips from time to time. As a result, the cell cycle dramatically disrupts the clock. In the *SI* we show that both of these effects survive the introduction of intrinsic noise in chemical reactions and of stochasticity in the timing of DNA replication (Figs. 2.E.1-2.F.1; see also Fig. 2.J.1). Fig. 2.3 qualitatively explains how locking arises in the NTFO.

2.2.3. A PHOSPHORYLATION CYCLE MAKES THE CLOCK MORE ROBUST AGAINST A TIME-VARYING GENE DENSITY

To study how a more realistic clock can become resilient to variability in the gene density, we turn to the *S. elongatus* circadian clock, and more specifically to the model of

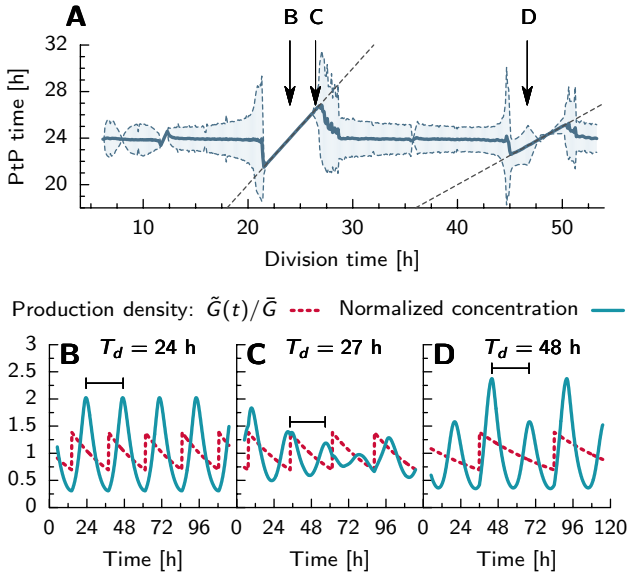

Figure 2.2: Periodic gene replication dramatically affects a negative transcriptional feedback oscillator (NTFO). (A) The average peak-to-peak time $\langle T_{\mathrm{PtP}} \rangle$ (solid curve) versus the cell division time T_{d} at fixed μ_{tot} and β. The shaded region shows the standard deviation of the peak-to-peak times (see *SI text*). Dashed lines indicate regions where the clock locks to the cell cycle with periods in a 1:1 (left) or 2:1 (right) ratio. (Smaller locking regions around $T_{\mathrm{d}} = 6, 12,$ and 36 h are not marked.) (B–D) Protein concentration $C(t)$ (blue solid line) and the protein production density $\tilde{G}(t) = g(t-\Delta)/V(t)$ (red dashed line) for the values of T_{d} indicated by the arrows in (A); horizontal brackets in (B–D) illustrate the definition of the peak-to-peak time T_{PtP}. At $T_{\mathrm{d}} = 24$ h (B), the clock locks firmly to the cell cycle. For $T_{\mathrm{d}} = 27$ h (C), the cell-cycle period is just too large for locking; as a result, the cell cycle dramatically disrupts the clock, leading to a large standard deviation of T_{PtP} (see panel A). At $T_{\mathrm{d}} = 48$ h (D), two oscillation cycles of the NTFO fit exactly in one division time. The larger amplitude oscillation cycle corresponds to cell cycle phases where $\tilde{G}(t)$ is higher and the smaller amplitude to phases where $\tilde{G}(t)$ is lower. Similar results are obtained upon varying T_{d} at constant μ_{act} (Fig. 2.G.1).

Zwicker *et al.* [15, 19] (Fig. 2.1F). This model provides a detailed description of the clock, including the synchronization of the phosphorylation state of different KaiC hexamers via KaiA sequestration and the coupling of the PPC oscillator to the TTC via RpaA. It represents KaiC as a hexamer but does not explicitly take into account that each KaiC monomer has two distinct phosphorylation sites [22, 60]. In the *SI Text*, Fig. 2.K.1, we show that a model based on that of Rust *et al.* [22], which describes KaiC at the level of monomers with two phosphorylation sites, gives similar results. We thus expect that still more elaborate models of the PPC, which include hexameric KaiC with two phosphorylation sites per monomer, such as our new model presented in chapter 4 and [18], will lead to similar results. To include gene replication, we modify the model of [19] so that the delayed negative feedback on KaiC production is modulated by a regularly oscillating

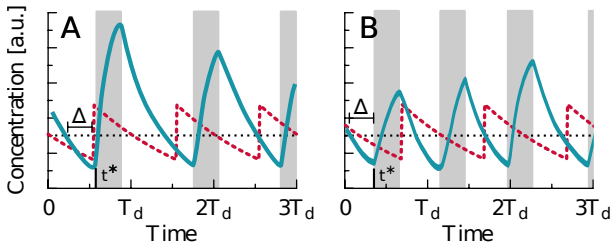

Figure 2.3: Locking mechanism for the NTFO. Shown are time courses of the production density $\tilde{G}(t) = g(t-\Delta)/V(t)$ (dashed red lines) and the protein concentration $C(t)$ (solid blue lines). For clarity, we consider the limit $n \to \infty$, in which the Hill function describing autoregulation (Eq. 2.2) reduces to a step function with repression threshold K_c, denoted by the dotted horizontal line. Shaded regions indicate times when $C(t)$ is rising. The panels correspond to two different initial phase differences between the NTFO and the cell cycle. In each case, when $C(t)$ drops below K_c at time $t^* - \Delta$, protein production starts, but because of the delay Δ, new molecules are injected into the system only at time t^*. (A) The gene has replicated just before $t^* - \Delta$, and $\tilde{G}(t^*)$ is hence large, yielding a large amplitude for the next NTFO cycle. Because the rate of protein decay is independent of $\tilde{G}(t)$, the period of the NTFO cycle is correspondingly long. The subsequent NTFO cycle thus begins at smaller $\tilde{G}(t^*)$, causing it to have a smaller amplitude and a shorter period. (B) The gene has not yet replicated at time $t^* - \Delta$, and $\tilde{G}(t^*)$ is therefore low; consequently, the amplitude and period of the next NTFO cycle are small. The beginning of the subsequent cycle is then shifted towards higher $\tilde{G}(t^*)$, increasing its period. In both cases, the result is that, after a few cell cycles, the period of the NTFO oscillation approaches that of the cell cycle, yielding stable 1:1 locking where the two oscillators have a well-defined phase relation. The largest amplitude and thus longest possible clock period arise when the protein synthesis phase (grey bar) coincides with the maximal $\tilde{G}(t^*)$; if T_d increases beyond this maximal period, locking cannot occur. An analogous loss of locking occurs if T_d decreases below the minimal possible clock period. In either case, the clock shows erratic behavior until T_d approaches values where 1:2 or 2:1 locking is possible.

protein production density $\tilde{G}(t)$ (see *SI Text*). We follow both the total KaiC concentration $C_{tot}(t)$ and the KaiC phosphorylation fraction $p(t) = \sum_{n=1}^{6} nC_n(t)/(6\,C_{tot}(t))$, where C_n is the concentration of n-fold phosphorylated KaiC hexamers.

Fig. 2.4A shows that a model with a PPC coupled to a TTC has a smaller locking window than an NTFO and lacks the large deviations in T_{PtP} just outside the locking region. The *S. elongatus* clock is hence more robust to gene replication than one based only on negative transcriptional feedback.

2.2.4. CLOCK READOUT THROUGH AN RPAA-BASED PUSH-PULL NETWORK FILTERS OUT CELL-CYCLE-DEPENDENT VARIATIONS IN PROTEIN CONCENTRATIONS

Although the variance of T_{PtP} outside of the locking region is relatively small for the combined TTC-PPC model, Fig. 2.4B shows that $C_{tot}(t)$ exhibits strong amplitude fluctuations, mirroring those observed for the NTFO (Fig. 2.2). The phosphorylation fraction $p(t)$, in contrast, is far more resilient, suggesting that the clock encodes temporal infor-

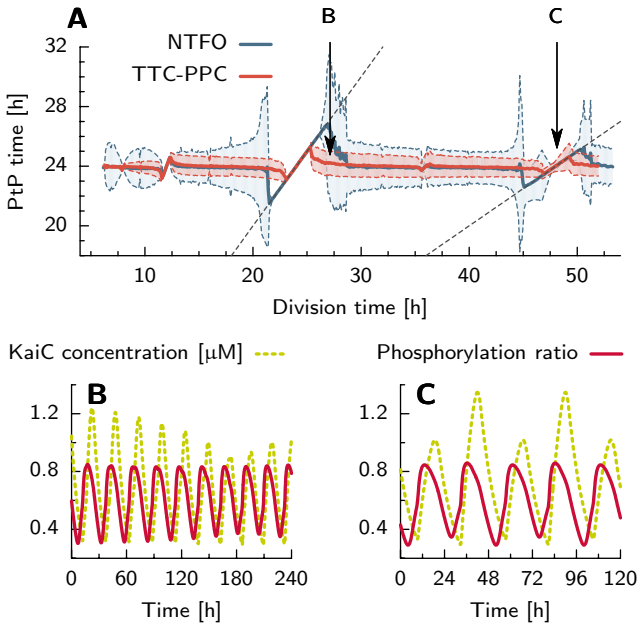

Figure 2.4: A clock with interlocked phosphorylation and transcriptional cycles is more robust against perturbations from periodic gene replication. (A) The average peak-to-peak times $\langle T_{\mathrm{PtP}} \rangle$ of the phosphorylation level $p(t)$ of the coupled TTC-PPC model of the Kai system [19] (red solid curve) and of $C(t)$ of the NTFO (solid blue curve, same as Fig. 2.2A), as a function of the cell division time T_{d}. The shaded regions show the standard deviation of T_{PtP}. Both the widths of the locking regions and the standard deviations of the peak-to-peak time outside the locking regions are smaller for $p(t)$ of the Kai system than for $C(t)$ of the NTFO. Arrows indicate division times for which we show time traces in (B,C). (B) The total KaiC concentration $C_{\mathrm{tot}}(t)$ (dashed line) and $p(t)$ (solid line) at $T_{\mathrm{d}} = 26$ h. Though the amplitude of $C_{\mathrm{tot}}(t)$ is strongly affected by gene replication, the amplitude of $p(t)$ is nearly constant. (C) Plots of $p(t)$ and $C_{\mathrm{tot}}(t)$ at $T_{\mathrm{d}} = 48$ h, where the amplitude of $C_{\mathrm{tot}}(t)$ alternates between a low and a high value depending on the gene copy number in the cell. In contrast, $p(t)$ is almost unaffected by gene replication.

mation more reliably in $p(t)$ than in $C_{\mathrm{tot}}(t)$. Intriguingly, the RpaA-centered push-pull network that transmits this timing signal to downstream genes [27, 54–57, 61] in fact responds primarily to $p(t)$: Because the rates of RpaA phosphorylation and dephosphorylation are indirectly controlled by different KaiC phosphoforms, variations in C_{tot} at fixed p change both rates together, leaving the fraction of phosphorylated RpaA largely unaffected. In contrast, changes in p shift the balance between the two opposing reactions and so modify the RpaA phosphorylation fraction (Fig. 2.H.1 and *SI text*). Thus, not only is the basic PPC-based timekeeping mechanism insulated from variations in protein synthesis, but the readout mechanism selectively follows this more robust signal.

2.2.5. MULTIPLE CHROMOSOME COPIES WEAKEN THE CELL CYCLE'S INFLUENCE ON THE CLOCK

While the PPC reduces gene replication's effect on the clock, it does not eliminate it entirely (Fig. 2.4). What other mechanisms might explain the observed resistance of the *S. elongatus* clock to the cell-cycle? It is known that *S. elongatus* has multiple, identical copies of its chromosome [58, 62–64]. These are not duplicated simultaneously, but rather one at a time, so that DNA replication occurs at a roughly constant rate throughout the cell cycle; furthermore, the timing of chromosome duplication appears to be independent of the phase of the clock [3, 58, 62, 64, 65]. Motivated by this observation, we consider a cell that starts with N chromosomes after division and let $g(t)$ rise to $2N$ in N evenly spaced steps (Fig. 2.5A–B). For larger N, the gene-copy number $g(t)$ increases more gradually, and hence the discrete jumps in the gene density $G(t)$ are considerably smaller. The effect on the clock is dramatic: in both the NTFO (solid line) and the TTC-PPC (dashed line), not only do the locked regions almost disappear for $N = 4$ (Fig. 2.5C), but the variance in the peak-to-peak time T_{PtP} becomes very small (Fig. 2.5D). This latter effect persists even when significant stochastic variability in the rhythm of gene replication (parameterized by the standard deviation σ_{rep} in the replication times —see *SI text*) is introduced. In fact, while *S. elongatus* can have as many as $N \approx 4$ chromosome copies at the beginning of the cell cycle [58, 62–64], these changes are already apparent when N is increased from 1 to 2 (Fig. 2.J.1).

2.3. DISCUSSION

Given the pleiotropic roles of both the cell cycle and the circadian clock, it is natural to ask whether they also influence each other. Our central observation is that such influence need not involve specific interactions between the core genes or proteins of the two systems [32, 39, 40]; rather, the simple fact that the number of cellular copies of a given gene necessarily experiences discrete jumps during DNA replication (Fig. 2.1) implies that clocks must in general feel a periodic driving from the cell cycle [41]. Whereas some genetic circuits can simply average over this time-varying input, oscillators—including biological clocks—are known to be especially sensitive to rhythmic forcing. Indeed, an NTFO either locks to the cell cycle or shows erratic oscillations for a range of doubling times T_{d} (Fig. 2.2), losing its ability to function as a clock in either case.

In light of this strong and detrimental coupling between the cell cycle and a simple transcriptional clock, it is all the more striking that the *S. elongatus* clock is so stable. Our analysis highlights two features of the cyanobacterial clock that are predicted to allow the necessary decoupling from the cell cycle. First, a time-varying gene dosage influences a clock with an autonomous post-translational oscillator less than it does a purely transcriptional clock; even *within* the combined TTC-PPC, the oscillations of the KaiC phosphorylation fraction $p(t)$ are less affected by periodic gene replication than are those of the total KaiC concentration $C_{\mathrm{tot}}(t)$ (Fig. 2.4, Fig. 2.F.1C). Strikingly, the RpaA-based push-pull network that communicates the clock state to the rest of the cell responds to p while ignoring the more strongly fluctuating C_{tot} (somewhat in the spirit of mechanisms that improve the robustness of bacterial chemotaxis to gene expression noise [66]). This filtering function of the push-pull architecture could help explain why the *S. elongatus*

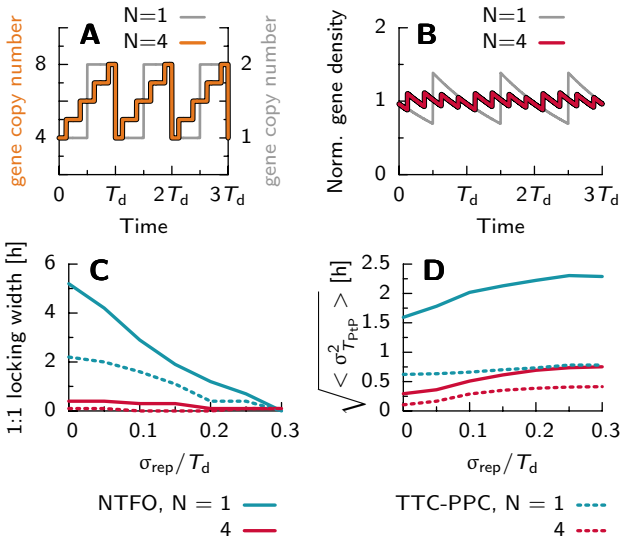

Figure 2.5: Multiple chromosome copies strongly reduce the cell cycle's effect on the circadian clock. (A) Gene copy number $g(t)$ for initial gene copy numbers $N = 4$ (thick curve, left axis) and $N = 1$ (thin curve, right axis) versus time (in units of cell cycle time T_d). The increase in $g(t)$ is more gradual for $N = 4$ than for $N = 1$. (B) The gene density $G(t) = g(t)/V(t)$, normalized to its time average, for $N = 4$ (thick curve) and $N = 1$ (thin curve). At a higher gene copy number, the deviations from the average gene density become smaller. The width of the 1:1 locking region (C) and the square root of the average variance in the peak-to-peak time (D) as a function of the standard deviation in the gene replication time σ_{rep} in a model where the times of replication events vary stochastically about their means (see *SI text*), for the NTFO (solid line) and the TTC-PPC [19] (dashed line). Increasing the chromosome copy number N reduces both the width of the locking region (C) and the variance in the peak-to-peak time (D). In contrast, while increasing σ_{dup} reduces the former, it increases the latter. See also Figs. 2.I.1 and 2.J.1.

clock has a relatively complex output mechanism requiring both CikA and SasA rather than a simpler linear design [67]. More generally, these results underscore the importance of the PPC in providing robustness to the clock [1, 19].

The second feature of the *S. elongatus* clock that we predict mitigates perturbations from the cell cycle is the presence of multiple, identical, asynchronously replicating chromosome copies [58, 62, 64, 65]. This reduces the importance of each individual gene replication event: Rather than seeing a single doubling of the number of gene copies each cell cycle, a cell with many chromosomes instead sees a number of smaller jumps that it can more easily ignore (Fig. 2.5). This adaptation may thus have evolved in part to protect the *S. elongatus* clock from cell cycle effects.

Whereas we have argued that the cell cycle generically affects any transcriptional clock, no comparably general mechanisms exist in the other direction. Moreover, though in many eukaryotic systems the clock is known to regulate key cell-cycle genes [3, 32–38, 68], no similar, specific connections have yet been characterized in *S. elongatus*. In par-

ticular, clock-dependent cell-cycle gating [3], because it acts on cell division but not on growth or DNA replication, does not allow the clock to block the discrete gene replication events that underlie the driving. Nonetheless, since the majority of *S. elongatus* genes shows some degree of clock-dependent expression [69], it is possible that the cyanobacterium's clock does regulate its cell cycle in some as yet undiscovered way. Any such coupling would however have to be weak enough to be consistent with the observation that the rhythm of DNA replication does not depend on clock phase [3, 58, 62, 64, 65]. Because phase locking between two oscillators has strong similarities to the locking of a single oscillator to periodic driving [48], most of our qualitative conclusions would remain unchanged in this case.

To isolate the behavior of the core, autonomous circadian oscillator, studies in the lab are typically performed at constant light levels. In keeping with this tradition, we have limited ourselves here to models of free-running clocks, without any diurnal environmental variation. In nature, however, the circadian clock is exposed to many additional entrainment signals, most notably the 24 h light-dark cycle. In fact, the environmental and cell cycle entrainment signals are intricately intertwined, because DNA replication and the synthesis of most proteins, including clock components, come to a standstill in the dark in a clock-independent fashion [65, 70]. We leave the effects of this complex interplay for future work.

Although we have focused on interactions between the cell cycle and the clock in *S. elongatus*, the basic idea that periodic gene replications must influence biological oscillators is more general and should apply to a wide range of prokaryotic and eukaryotic species. Indeed, cell-cycle-dependent changes in gene copy number have clearly observable effects on gene expression in eukaryotic cells [45], and recent experiments in cultured metazoan cells strongly suggest that the cell cycle exerts a considerable influence on the circadian clock, generally leading to phase locking of the two oscillators [39, 40]. Other generic forms of driving from the cell cycle may also play a role here: for example, in contrast to prokaryotes, eukaryotes typically shut down transcription around mitosis, thereby introducing another source of periodic, cell-cycle dependent variation in protein synthesis [32, 39, 40]. Our analysis thus highlights an important constraint on the design of circadian clocks in organisms from bacteria to humans.

Further, there is no reason for the effects of regular, discrete gene replications to be limited to circadian clocks; they should be observable in any cellular oscillator that depends on transcription and has a period on the same order as that of the cell cycle. Thus, our results may be relevant to phenomena like coupling between the cell cycle and the segmentation clock in vertebrate development [71]. Similarly, in chapter 3 we show that two well-known synthetic circuits [28, 29] can also lock to the cell cycle, and that the strength of locking depends sensitively on the oscillator architecture.

Since we have argued that *S. elongatus* possesses particular adaptations that decouple its circadian clock from the cell cycle, the most obvious experimental test of our ideas would be to observe the consequences of blocking or removing these features. Several strains already exist that might allow just such experiments. Mutants of *S. elongatus* are known with significantly fewer chromosomes per cell than the wildtype [72]; moreover, in some other *Synechococcus* strains, cells are always monoploid [63]. We find that in cells where the number of chromosomes goes from 1 to 2 over the course of a single di-

vision cycle, it should be possible to observe clear signatures of driving by the cell cycle in plots of KaiC's abundance—but not its phosphorylation level—as a function of time (Fig. 2.4). We predict that this effect will be further strengthened if the PPC is removed entirely. It is well-established that this can be accomplished by hyper-phosphorylating KaiC [53, 73]. In all cases, one could study forcing by the cell cycle at a variety of different doubling times. We suggest, however, that a doubling time near 48 hours offers a particularly unambiguous signature of the cell cycle's influence: The KaiC abundance as a function of time should then rise and fall every 24 hours, with successive peaks strictly alternating between higher and lower levels (Fig. 2.4C).

APPENDIX

2.A. OVERVIEW OF MODELS AND NOMENCLATURE

This Supporting Information (SI) discusses three different models of a circadian clock driven by periodic gene replication, which we list here to summarize our naming conventions and the distinctions among the models:

- The Negative Transcriptional Feedback Oscillator, or **NTFO**, consists of a single gene that negatively regulates its own transcription with a delay. Because of gene replication, the number of copies of this gene in each cell doubles over the course of a cell cycle (as described in the next section and in the main text).
- We refer to our central model of the *S. elongatus* circadian clock as either the **TTC-PPC** model or the **TTC-(PPC$_{\text{Zwicker}}$)** model, with the latter name reserved for those parts of this *SI* where there is potential for confusion with the **TTC-(PPC$_{\text{Rust}}$)** model (next item). The **TTC-(PPC$_{\text{Zwicker}}$)** model consists of the protein phosphorylation cycle (PPC) model of Van Zon *et al.* [15] joined to a transcription-translation cycle (TTC) as in the work of Zwicker *et al.* [19] and subject to periodic driving from the cell cycle because of gene replication, as discussed in the main text.
- We also present results for the **TTC-(PPC$_{\text{Rust}}$)** model, which couples the description of the PPC proposed by Rust *et al.* [22] to the same models of the TTC and of forcing from the cell cycle used in the **TTC-(PPC$_{\text{Zwicker}}$)** model.

Of these models, the first two (NTFO and TTC-(PPC$_{\text{Zwicker}}$)) are discussed in the main text, while the third (TTC-(PPC$_{\text{Rust}}$)) is introduced in this Appendix, to demonstrate that our major qualitative conclusions do not depend on our specific assumptions about the PPC.

2.B. THE DETERMINISTIC NEGATIVE TRANSCRIPTIONAL FEEDBACK OSCILLATOR (FIGS. 2.2 AND 2.4)

Here we describe the negative transcriptional feedback oscillator, NTFO, studied in the main text, together with its parameters. The model consists of a single variable, $C(t)$, describing the concentration of proteins that inhibit their own production:

$$\frac{dC(t)}{dt} = \beta \tilde{G}(t) \frac{K_c^n}{K_c^n + C(t-\Delta)^n} - \mu_{\text{tot}} C(t). \tag{2.3}$$

We impose a fixed delay Δ between the initiation of transcription and the appearance of functional proteins. Therefore, protein production at time t is proportional to the gene copy number $g(t-\Delta)$ at time $t-\Delta$. These proteins enter the cell volume $V(t)$ at time t.

Combining these two effects, the protein synthesis rate per unit volume at time t is thus proportional to the *protein production density* $\tilde{G}(t) \equiv g(t-\Delta)/V(t)$. Because the production at time t depends on the state of the promoter at $t-\Delta$, the Hill function describing auto-regulation with Hill coefficient n and concentration of half-maximal repression K_c, is evaluated with the delayed concentration $C(t-\Delta)$. Proteins are degraded with a total rate $\mu_{\rm tot} = \mu_{\rm d} + \mu_{\rm act}$, where $\mu_{\rm d}$ describes dilution due to cell growth, and $\mu_{\rm act}$ describes possible active degradation. Including both terms allows us to vary the doubling time $T_{\rm d}$ while holding $\mu_{\rm tot}$ constant and hence to distinguish the trivial influence of the cell cycle on the clock through the dilution rate $\mu_{\rm d}$ from other effects. This model is a deterministic one, based on mean-field chemical rate equations. A stochastic version that takes into account the intrinsic stochasticity of biochemical reactions is introduced further below.

Parameters used in the simulations are: $\beta = 6.0 \cdot 10^3 \mathrm{h}^{-1}$; $K_c = 1.0\mu\mathrm{M}$; $n = 2$; $\mu_{\rm tot} = 0.2\mathrm{h}^{-1}$; $\Delta = 8\mathrm{h}$. Details regarding the simulations are given in the Methods section of this document. The principal results of this model are presented in Figs. 2 and 4 of the main text.

2.C. THE TTC-(PPC$_{\rm Zwicker}$) MODEL (FIGS. 2.4 AND 2.5)

The TTC-PPC model of the main text is built on the TTC-PPC model of Zwicker *et al.*. It consists of a protein phosphorylation cycle (PPC) combined with a transcription-translation cycle (TTC) [19]. The PPC model is based on that of Van Zon *et al.* [15]. In this model, each KaiC hexamer has an intrinsic tendency to progress through a phosphorylation cycle, while the phosphorylation cycles of the individual hexamers are synchronized via the mechanism of differential affinity: KaiA stimulates KaiC phosphorylation, but the limited supply of KaiA binds preferentially to those KaiC hexamers that are falling behind in the cycle, forcing the front runners to slow down and allowing the laggards to catch up. The model includes the following reactions [15]:

$$\mathrm{C}_i \underset{b_i}{\overset{f_i}{\rightleftarrows}} \widetilde{\mathrm{C}}_i, \qquad \mathrm{C}_i + \mathrm{A} \underset{k_i^{\rm Ab}}{\overset{k_i^{\rm Af}}{\rightleftarrows}} \mathrm{AC}_i \overset{k_{\rm pf}}{\to} \mathrm{C}_{i+1} + \mathrm{A}, \tag{2.4}$$

$$\widetilde{\mathrm{C}}_i + \mathrm{B} \underset{\tilde{k}_i^{\rm Bb}}{\overset{2\tilde{k}_i^{\rm Bf}}{\rightleftarrows}} \mathrm{B}\widetilde{\mathrm{C}}_i, \qquad \mathrm{B}\widetilde{\mathrm{C}}_i + \mathrm{B} \underset{2\tilde{k}_i^{\rm Bb}}{\overset{\tilde{k}_i^{\rm Bf}}{\rightleftarrows}} \mathrm{B}_2\widetilde{\mathrm{C}}_i, \tag{2.5}$$

$$\mathrm{B}_x\widetilde{\mathrm{C}}_i + \mathrm{A} \underset{\tilde{k}_i^{\rm Ab}}{\overset{x\tilde{k}_i^{\rm Af}}{\rightleftarrows}} \mathrm{AB}_x\widetilde{\mathrm{C}}_i, \qquad \mathrm{AB}_2\widetilde{\mathrm{C}}_i + \mathrm{A} \underset{2\tilde{k}_i^{\rm Ab}}{\overset{\tilde{k}_i^{\rm Af}}{\rightleftarrows}} \mathrm{A}_2\mathrm{B}_2\widetilde{\mathrm{C}}_i, \tag{2.6}$$

$$\mathrm{C}_i \underset{k_{\rm dps}}{\overset{k_{\rm ps}}{\rightleftarrows}} \mathrm{C}_{i+1}, \qquad \widetilde{\mathrm{C}}_i \underset{\tilde{k}_{\rm dps}}{\overset{\tilde{k}_{\rm ps}}{\rightleftarrows}} \widetilde{\mathrm{C}}_{i+1}, \tag{2.7}$$

$$\mathrm{B}_x\widetilde{\mathrm{C}}_i \underset{\tilde{k}_{\rm dps}}{\overset{\tilde{k}_{\rm ps}}{\rightleftarrows}} \mathrm{B}_x\widetilde{\mathrm{C}}_{i+1}, \qquad \mathrm{A}_y\mathrm{B}_x\widetilde{\mathrm{C}}_i \underset{\tilde{k}_{\rm dps}}{\overset{\tilde{k}_{\rm ps}}{\rightleftarrows}} \mathrm{A}_y\mathrm{B}_x\widetilde{\mathrm{C}}_{i+1}\,. \tag{2.8}$$

Here, C_i denotes a KaiC hexamer in the active conformational state, in which the number i of phosphorylated monomers tends to increase, and $\widetilde{\mathrm{C}}_i$ denotes a KaiC hexamer in the inactive conformational state in which i tends to decrease; A denotes a KaiA dimer,

and B denotes a KaiB dimer. The reactions $C_i \rightleftarrows \widetilde{C}_i$ in Eq. 2.4 model the conformational transitions between active and inactive KaiC; the second set of reactions in Eq. 2.4 describe phosphorylation of active KaiC that is stimulated by KaiA. The reactions in Eq. 2.5 model the binding of KaiB to inactive KaiC, and those in 2.6 model the sequestration of KaiA by inactive KaiC that is bound to KaiB; note that in this model an inactive KaiC hexamer can bind up to two KaiA dimers. The reactions in Eqs. 2.7 and 2.8 model spontaneous phosphorylation and dephosphorylation of active and inactive KaiC. For a more detailed discussion of the model, we refer to [15].

The TTC and the coupling between the PPC and TTC are described by the following reactions:

$$\widetilde{R} + X \xrightarrow{k_a} R + X, \qquad R + \widetilde{X} \xrightarrow{k_i} \widetilde{R} + \widetilde{X}, \tag{2.9}$$

$$\emptyset \overset{\beta \tilde{G}(t)[R]^4/(K^4+[R]^4)}{\underset{\tau}{\Longrightarrow}} C_6 + 3B, \qquad \emptyset \xrightarrow{\beta_a} A,\ \emptyset \xrightarrow{\beta_r} \widetilde{R}, \tag{2.10}$$

$$R, \widetilde{R}, A, B, AC_i, B_x\widetilde{C}_i, A_yB_x\widetilde{C}_i \xrightarrow{\mu} \emptyset\,. \tag{2.11}$$

Here, R and $\widetilde{R}$ denote the RpaA protein in its active and its inactive form, respectively. The X and $\widetilde{X}$ in Eq. (2.9) denote any of the phosphoforms of KaiC that mediate the activation and repression of RpaA, respectively; as described in more detail in [19], KaiC in the phosphorylation phase activates RpaA, while KaiC in the dephosphorylation phase deactivates it. The double arrow indicates a reaction with a fixed delay τ; we use τ rather than Δ to denote the delay to agree with the notation of [19]. We thus assume that *kaiBC* expression is activated by RpaA and that the activity of RpaA is modulated by the PPC. In contrast, the expression of KaiA and RpaA is taken to occur constitutively. The effect of gene replication is included by making the rate of C_6 production dependent on $\tilde{G}(t)$, just as in the NTFO. We use the parameters given in the supplementary information of [19], except for: $\beta = 1.02 \cdot 10^2 \mathrm{h}^{-1}$ and $\mu_{\mathrm{tot}} = 0.1\mathrm{h}^{-1}$. As for the NTFO, we keep the total degradation rate constant, so that we can distinguish the effects of protein dilution from those due specifically to periodic gene replication events.

2.D. THE TTC-($\mathrm{PPC_{Rust}}$) MODEL (FIG. 2.K.1)

We argue in the main text that entrainment of circadian clocks by the cell cycle should be a robust, generic phenomenon that does not depend on the precise model studied. In support of this claim, we here present a model of the Kai system, the TTC-($\mathrm{PPC_{Rust}}$) model, that combines the TTC of Zwicker *et al.* [19] with a model of the PPC developed by Rust and coworkers [22]; this model is here extended to include a description of the cell cycle with periodic gene replication. The PPC model of Rust *et al.* describes the PPC at the level of KaiC monomers, rather than of hexamers, as in the models of Van Zon *et al.* and Zwicker *et al.* considered in the preceding section and in the main text [15, 19]. The monomers go through a sequence of 4 different phosphorylation states —unphosphorylated (U), phosphorylated only on threonine 432 (T), doubly phosphorylated (D), and phosphorylated only on serine 431 (S)—in a 24 hour cycle [60]. As detailed in the supplementary information of [19], we extended the original Rust model, which contains only the PPC, to include a transcription-translation cycle. Here, we briefly describe the model and discuss how it responds to forcing from the cell cycle.

This PPC is described by the reactions

$$\mathrm{U} \leftrightarrow \mathrm{T}, \qquad \mathrm{T} \leftrightarrow \mathrm{ST}, \qquad \mathrm{ST} \leftrightarrow \mathrm{S}, \qquad \mathrm{S} \leftrightarrow \mathrm{U} \tag{2.12}$$

with reaction rates given by Eq. 5 of the supplementary material of Rust *et al.* [22]. These rates depend on the concentration of free KaiA, which is sequestered by KaiC in the S-state. We model KaiA sequestration explicitly:

$$\mathrm{S} + \mathrm{A} \leftrightarrow \mathrm{AS}, \qquad \mathrm{AS} + \mathrm{A} \leftrightarrow \mathrm{A_2S}. \tag{2.13}$$

Dephosphorylation of KaiC in the S-state is allowed to occur even when KaiA is bound, in which case the KaiA protein is released from the complex. We define the output signal as

$$p(t) = \frac{[\mathrm{T}] + [\mathrm{ST}] + [\mathrm{S}] + [\mathrm{AS}] + [\mathrm{A_2S}]}{[\mathrm{U}] + [\mathrm{T}] + [\mathrm{ST}] + [\mathrm{S}] + [\mathrm{AS}] + [\mathrm{A_2S}]}, \tag{2.14}$$

which resembles the phosphorylation ratio in the case where we cannot distinguish between singly and doubly phosphorylated KaiC. The denominator in the above expression is also the total KaiC monomer concentration. We use the same total protein concentrations as Rust *et al.*, [KaiA] = 1.3 μM (active KaiA monomers) and [KaiC] = 3.4 μM (KaiC monomers).

The TTC is modeled as:

$$\emptyset \overset{\beta\tilde{G}(t)[\mathrm{R}]^4/(K^4+[\mathrm{R}]^4)}{\underset{\tau}{\Longrightarrow}} \mathrm{ST}, \quad \emptyset \xrightarrow{\beta_a} \mathrm{A}, \emptyset \xrightarrow{\beta_r} \widetilde{\mathrm{R}}, \tag{2.15}$$

$$\widetilde{\mathrm{R}} + \mathrm{T} \xrightarrow{k_a} \mathrm{R} + \mathrm{T}, \quad \mathrm{R} + \mathrm{A}_x\mathrm{S} \xrightarrow{k_i} \widetilde{\mathrm{R}} + \mathrm{A}_x\mathrm{S}, \qquad x \in \{0,1,2\}, \tag{2.16}$$

$$\mathrm{A}, \mathrm{R}, \widetilde{\mathrm{R}}, \mathrm{U}, \mathrm{S}, \mathrm{A}_x\mathrm{S}, \mathrm{T}, \mathrm{ST} \xrightarrow{\mu} \emptyset. \tag{2.17}$$

The first line describes protein production and decay; as in Eq. 2.11, the double arrow indicates a delayed reaction. The second line summarizes the RpaA signaling pathway, where KaiC that is phosphorylated at the T site activates RpaA and KaiC that is phosphorylated at the S site represses RpaA activation.

As in our other models, we introduced the effect of gene replication by making the production rate of KaiC proportional to the production density $\tilde{G}(t)$. We use the parameters given in [22] and in section S5.2 of the supplementary information of [19], except for $\beta = 1.29 \cdot 10^3 \mathrm{h}^{-1}$ and $\mu_{\mathrm{tot}} = 0.1 \mathrm{h}^{-1}$.

Fig. 2.K.1 shows the peak-to-peak times of the phosphorylation fraction of this model as a function of the cell-division time T_d. Clearly, this TTC-(PPC$_{\mathrm{Rust}}$) model, which combines a TTC with a PPC based on the model of Rust *et al.* [22], responds to forcing from the cell cycle in essentially the same way as the TTC-(PPC$_{\mathrm{Zwicker}}$) model [19], which couples the same TTC with a PPC based on the model of Van Zon and Zwicker *et al.* [15, 19]. This supports the idea that the benefit of a self-contained protein-modification oscillator is a generic feature of biological clocks.

2.E. THE NEGATIVE TRANSCRIPTIONAL FEEDBACK OSCILLATOR WITH INTRINSIC NOISE (FIG. 2.E.1)

To test the effect on the locking mechanism of intrinsic noise in the chemical reactions that constitute the circadian clock, we simulate the negative transcriptional feedback oscillator (NTFO) using kinetic Monte Carlo simulations of the chemical master equation. Eq. 2.2 of the main text implies that when this intrinsic noise is neglected, the number of proteins N_C in the cell obeys

$$\frac{dN_C(t)}{dt} = \beta g(t-\Delta)\frac{K_C^2}{K_C^2 + \left(\frac{N_C(t-\Delta)}{V(t)}\right)^2} - \mu_{act} N_C(t). \tag{2.18}$$

Here, $V(t)$ is the cell volume, which grows exponentially as described in the main text, and μ_{act} is the active contribution to the total decay rate $\mu_{tot} = \mu_{act} + \mu_d$ in Eq. 2; the term μ_d contributes to the total apparent decay rate for the protein concentration, but not for the protein number. To include the effects of intrinsic noise on the evolution of N_C, we adapted the standard kinetic Monte Carlo algorithm to take into account delayed reactions, volume growth, and gene replication, as described in [19]: The cell volume is increased at discrete time intervals, and reaction propensities are re-calculated after each volume update. After each cell division, the protein number N_C is chosen from a binomial distribution, with N_C halved on average. Gene replication is included through the time dependence of the gene copy number $g(t)$, whose behavior is detailed in the main text.

The parameters used in the simulation are: $\beta = 6.0{\cdot}10^3 \mathrm{h}^{-1}$; $K_c = 1.0\mu$M; $n = 2$; $\Delta = 8$h. The time average $\bar{V}$ of the cell volume is chosen to be $1\mu\mathrm{m}^3$. For different cell division times T_d, we change the active degradation rate such that the total decay rate is kept constant at $0.2\mathrm{h}^{-1}$: $\mu_{act} = 0.2\mathrm{h}^{-1} - \log(2)/T_d$. As in the main text, this allows us to disentangle the effect of gene replication on locking from that of simple protein dilution.

We vary the cell division time T_d from 6 to 52 hours in 0.1 hour intervals and simulate a single trajectory of 10,000 hours for each T_d. From the trajectories, we extract the peak-to-peak times of the oscillations (see Methods in this document). Fig. 2.E.1 shows the average peak-to-peak time of the stochastic NTFO model for different values of the cell division time, with initial gene copy number $N = 1$. Two differences from Fig. 2.2 of the main text, where the system obeys deterministic equations, are worthy of note: First, the 1:1 locking region is much larger when intrinsic noise is included, while the width of the 2:1 locking region has decreased. Intrinsic noise can thus dramatically change the extent of locking. We leave a full investigation of the origins of this effect for future work. Second, because of intrinsic noise, the amplitude is considerably more variable, and the variances in the peak-to-peak times outside of the locking regions are much larger. As in the mean-field model, the variances are very small around $T_d = 24$ hrs, due to locking.

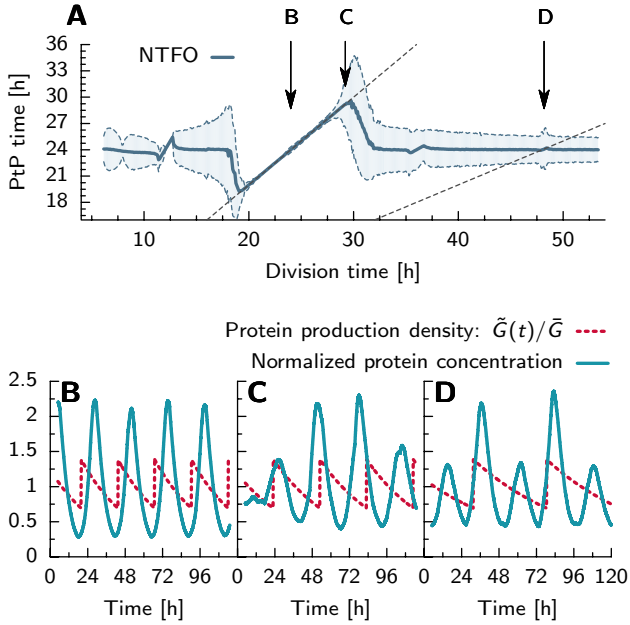

Figure 2.E.1: The effect of intrinsic noise on the locking of the negative transcriptional feedback oscillator (NTFO) to the cell cycle. (A) Average (solid line) and standard deviation (shaded region) of the peak-to-peak time T_{PtP} as a function of the division time T_{d} for an NTFO with intrinsic noise and initial gene copy number $N = 1$. The region of 1:1 locking with the cell cycle (left dashed line) has widened considerably compared to the deterministic case (Fig. 2.2A of the main text), and the standard deviation in T_{PtP} outside the locking region has increased. In contrast, the region of 2:1 locking (right red dashed line) has shrunk almost to nothing. (B–D) Representative time traces for the division times indicated by the arrows in panel A. Shown are the protein concentration $C(t) = N_C(t)/V(t)$ of the NTFO (blue solid line) and the protein production density $\tilde{G}(t)$ (red dashed line), both normalized by their time average values. At a division time of $T_{\mathrm{d}} = 24$h (B), the NTFO is locked to the cell cycle. Because of the intrinsic noise, the amplitude varies slightly from one oscillation cycle to the next. At $T_{\mathrm{d}} = 27$ h (C), just outside the locking region, the oscillator exhibits irregular behavior. At $T_{\mathrm{d}} = 48$ h (D), the NTFO oscillations switch between a small and a large amplitude in successive oscillation cycles, just as in the deterministic case.

2.F. THE EFFECT OF NOISE IN THE TIMING OF GENE REPLICATION EVENTS (FIG. 2.F.1)

In the model of the cell cycle described in the main text, gene replication events occur at perfectly regular, evenly spaced intervals in time. In this section, we explore how stochastic variability in the timing of these replications affects the interaction between the cell cycle and other oscillators. We consider a model in which each gene replicates exactly once in each cell division cycle, at a time t_{g} between 0 and T_{d}, where T_{d} is the length of the cell cycle and does not vary. The times t_{g} are drawn in each cell cycle independently from a Gaussian distribution of mean $\bar{t}_{\mathrm{rep}} = T_{\mathrm{d}}/2$ and variance σ^2_{rep}.

Replication times t'_g that fall outside the interval $[0, T_d)$, are mapped back onto it via $t_g = \mathrm{Mod}(t'_g, T_d)$.

We assume that the standard deviation in the gene replication times, σ_{rep}, is proportional to the cell division time: $\sigma_{rep} \propto T_d$. Because this quantity is, to our knowledge, not known for *S. elongatus*, we varied this quantity between zero and a value that corresponds to replication times being chosen randomly from a uniform distribution, $\sigma_{rep}/T_d = 1/\sqrt{12} \approx 0.3$.

Fig. 2.F.1 shows the effects of introducing this variability on the behavior of our clock models. For the NTFO (Fig. 2.F.1A), the locking regions are reduced in size, but still clearly noticeable. The variance in the peak-to-peak times is typically larger than in deterministic case. For the TTC-($\mathrm{PPC}_{\mathrm{Zwicker}}$) model [19] (Fig. 2.F.1B), the locking regions have almost disappeared, but the variance in T_{PtP} is nearly unaffected by the noise in the timing of gene replication. Panel C shows representative time traces of the total KaiC concentration, $C_{tot}(t)$ and the phosphorylation fraction $p(t)$, for $T_d = 48$h. Clearly, $C_{tot}(t)$ shows much more variability in the height of its peaks than does $p(t)$, further demonstrating the value of a post-translational oscillator in insulating a circadian clock from influences from the cell cycle. We also note that, as in the deterministic limit, the amplitude of the C_{tot} oscillation cycles still (despite the noise) alternates between a high and a low value when gene replications occur only once every 48 hours. It should thus be possible to observe experimentally that $C_{tot}(t)$ is markedly affected by periodic gene replication, while $p(t)$ is much less so.

2.G. ALLOWING THE PROTEIN DECAY RATE TO VARY WITH GROWTH RATE (FIG. 2.G.1)

The total protein decay rate μ_{tot} depends on the rate of active protein degradation μ_{act} and on the rate of dilution due to cell growth μ_d. In the results shown in the main text, we adjusted the active degradation rate with the growth rate so that the total protein decay rate remained constant—this allowed us to zoom in on the effect of locking that is due to periodic gene replication while ignoring confounding changes to clock behavior that might arise because of the variation of μ_{tot}.

It is entirely possible, however, that the real clock system in *S. elongatus* is actually closer to the opposite limit, in which μ_{act} is fixed and μ_d and μ_{tot} vary together with the division time T_d. To investigate how this affects the locking mechanism, we performed simulations in which we kept the active degradation rate μ_{act} constant, but allowed the total degradation rate μ_{tot} to vary with the cell-divisition time: $\mu_{tot} = \mu_{act} + \ln(2)/T_d$; upon varying μ_{tot}, we adjusted the protein synthesis rate β to keep the oscillation period at 24 h. The result is shown in Fig. 2.G.1. Just as in the case in which μ_{tot} is fixed, the effect of locking is very pronounced, both for a simple NTFO (panel A) and for a clock incorporating both a TTC and a PPC (panel B).

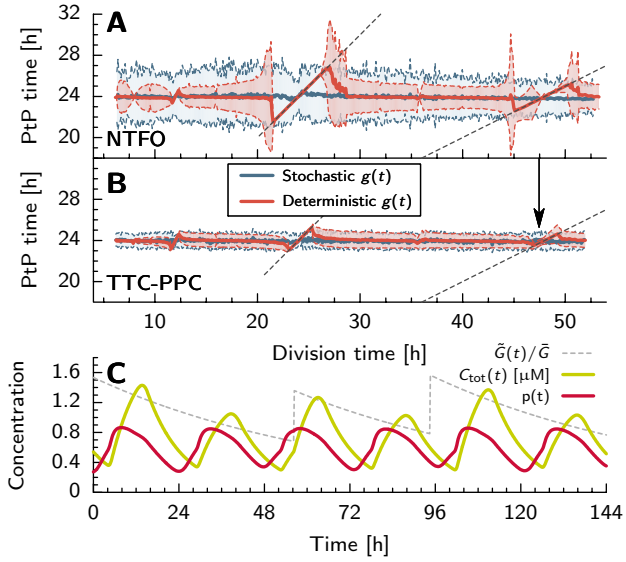

Figure 2.F.1: The effect of stochasticity in the timing of gene replication on locking to the cell cycle. (A) The average and variance of T_{PtP} for an NTFO in which the timing of gene replication is deterministic (red) or is drawn from a Gaussian distribution with a width σ that is 30% of the cell-division time T_{d}(blue). The stochasticity in the replication times decreases the width of the locking regions, but increases the variance in the peak-to-peak times. (B) Same as A, but for T_{PtP} of the phosphorylation fraction $p(t)$ of the TTC-(PPC$_{\mathrm{Zwicker}}$) model [19] (see *SI* section *The TTC-(PPC$_{\mathrm{Zwicker}}$) model*)[19]. Again, stochasticity in the timing of replication reduces locking, but in this case, the increase in the variance of T_{PtP} outside the locking region is much less marked. We attribute this to the ability of the PPC to insulate the clock from variability in gene expression levels. (C) Representative time traces of the production density $\tilde{G}(t)$ (normalized to its time average), the phosphorylation fraction $p(t)$, and the total KaiC concentration $C_{\mathrm{tot}}(t)$ for the Zwicker model for T_{d}=48h. As in the deterministic limit, the amplitude of the $C_{\mathrm{tot}}(t)$ oscillations tends to alternate between a high and a low value, due to gene replication occuring every 48 hours, on average; in contrast, the amplitude of $p(t)$ is relatively constant. The effect of periodic gene replication on $C_{\mathrm{tot}}(t)$ should thus be observable experimentally.

2.H. HOW DOES THE CELL READ OUT THE PHOSPHORYLATION FRACTION INSTEAD OF THE CONCENTRATION OF KAIC? (FIG. 2.H.1)

Both Fig. 2.4 and a comparison of the blue lines in Figs. 2.F.1A,B show that a circadian clock with a post-translational oscillator is much more robust to a time-varying gene density than is an NTFO. Both the peak-to-peak time and the amplitude of the phosphorylation fraction $p(t)$ of the TTC-PPC vary considerably less not just than the corresponding quantities for the NTFO, but even than those for the total protein concentration $C_{\mathrm{tot}}(t)$ of the TTC-PPC itself. To take advantage of the relative stability of the

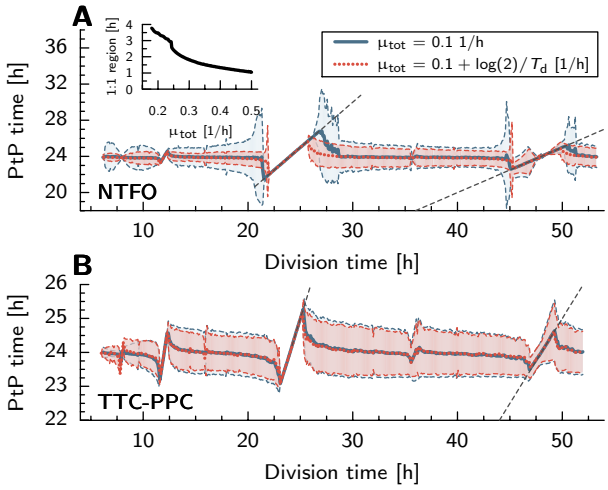

Figure 2.G.1: The effect of allowing the total protein decay rate μ_{tot} to vary with the cell-division time T_{d}, both for an NTFO (A) and for the TTC-(PPC$_{\mathrm{Zwicker}}$) model [19] of a clock, which combines a TTC with a PPC (B; note the vertical scale is different than in panel A). The blue lines correspond to the scenario in which the the total degradation rate is kept constant at $\mu_{\mathrm{tot}} = 0.1/\mathrm{h}$ (as in Figs. 2A and 4A of the main text), and the red lines to the scenario in which the total degradation rate depends on the division time as $\mu_{\mathrm{tot}} = 0.1\mathrm{h}^{-1} + \log(2)/T_{\mathrm{d}}$ [1/h]. When μ_{tot} depends on T_{d}, we adjust the KaiC production rate β such that the intrinsic period of the clock remains 24 hours. For both clock models and both choices of μ_{tot}, the clock tends to lock to the cell cycle. The difference between the results of the two protein-decay scenarios in the case of the NTFO can be understood by noticing that we have chosen our rates so that μ_{tot} never drops below 0.1 h^{-1} in either case, but can become larger than this bound when it is allowed to depend on T_{d}. The protein synthesis rate β then becomes higher than when μ_{tot} is constant. The higher synthesis and decay rate raises the amplitude of the concentration oscillations, making the clock more stable. As the inset indicates, the width of the locking region decreases with increasing μ_{tot} in a similar fashion when μ_{tot} does not depend on T_{d}. The TTC-PPC is almost insensitive to the higher degradation and production rates.

oscillation in $p(t)$, the cell needs to read out the phosphorylation fraction in a way that is insensitive both to the total concentration of KaiC and to the absolute concentrations of its specific phosphorylation states. How does it accomplish this?

To find out, we looked at the architecture of the biochemical network in *S. elongatus* that allows the clock to regulate the transcription of downstream genes. The temporal information encoded in the dynamics of the clock proteins is transmitted via a central node, the response regulator RpaA. This protein can be phosphorylated, and it is known that the phosphorylation level of RpaA controls the expression not only of core clock components, but also of a small set of genes that, in turn, direct genome-wide circadian rhythms [54, 57]. The phosphorylation state of RpaA is regulated by a push-pull network consisting of the histidine kinases SasA, which acts primarily to phosphorylate RpaA, and CikA, whose primary function is to dephosphorylate it [54–56]. The activi-

ties of SasA and CikA are in turn controlled by the different phosphorylation states of KaiC, such that KaiC proteins that are in the phosphorylation phase of the clock tend to push up the phosphorylation level of RpaA [27, 54], while those that are in the clock's dephosphorylation phase tend to pull down RpaA's phosphorylation level [27, 55]. Recent experiments suggest that a structural change in KaiB, which binds KaiC during its dephosphorylation phase, might play a key role in this switch, by simultaneously blocking SasA from binding to KaiC and engaging CikA [27].

To show that such a push-pull network makes the clock readout, the RpaA phosphorylation level, sensitive to the KaiC phosphorylation fraction $p(t)$, but not to its concentration $C_{\mathrm{tot}}(t)$, we adapted the canonical model of Goldbeter and Koshland [61]. A cartoon of the model is shown in Fig. 2.H.1B. It consists of a substrate S, playing the role of RpaA, which can be phosphorylated and dephosphorylated by the antagonistic enzymes K and P, corresponding respectively to SasA and CikA, each of which can be in active (K^* and P^*) or inactive states. Transitions between these states are governed by the time-dependent forward rates $k_K(t)$ and $k_P(t)$, which mimic the effects of time-varying concentrations of different KaiC phosphoforms. In our model, KaiC in the phosphorylation phase increases $k_K(t)$, while KaiC in the dephosphorylation phase increases $k_P(t)$. The substrate-modification reactions follow the standard Michaelis-Menten schemes $K^* + S \rightleftharpoons K^*S \rightarrow K^* + S_p$ and $P^* + S_p \rightleftharpoons P^*S_p \rightarrow P^* + S$.

The key question is whether the phosphorylation level of RpaA depends only on the phosphorylation fraction of KaiC, $p(t)$, or whether it is also significantly affected by the total concentration of KaiC. In terms of the model just presented, we must thus ask whether $[S_p]/[S_{\mathrm{tot}}]$ (the fraction of phosphorylated RpaA) is sensitive only to the *ratio* $k_K(t)/k_P(t)$ or whether it depends on the two rates individually. We begin by considering this question for the case of time-independent rates, in which case the ratio of total concentrations of the active enzyme forms $[K^*]/[P^*]$ is proportional to $k_K(t)/k_P(t)$ and may be used in its place. In qualitative terms, it is easy to imagine that, since K^* and P^* have opposite effects, increasing the concentration of each one by the same factor might speed up the reaction kinetics but would not affect the steady state ratio $[S_p]/[S_{\mathrm{tot}}]$. Indeed, in the regime that the concentrations of the complexes K^*S and P^*S_p are negligible compared to the concentrations of free S and S_p, we can equate the rates of S phosphorylation and dephosphorylation in steady state to arrive at a relation of the form

$$\frac{k_+[K^*][S]}{K_{M,+}+[S]} = \frac{k_-[P^*][S_p]}{K_{M,-}+[S_p]}\,. \tag{2.19}$$

Together with the conservation law $[S]+[S_p]=[S_{\mathrm{tot}}]$, this equation can easily be solved to give $[S_p]/[S_{\mathrm{tot}}]$ as a function of $[K^*]/[P^*]$ only. It is possible, however, that in the RpaA system the concentrations of the intermediate complexes K^*S and P^*S_p cannot be neglected. Fig. 2.H.1A shows that even in this case, to a very good approximation the steady state phosphorylation fraction of S depends only on the ratio $[K^*]/[P^*]$. This mechanism, by which the output of a push-pull network depends on the ratio of the concentrations of the two antagonistic enzymes, but not on their absolute values, has previously been invoked to explain the robustness of the *E. coli* chemotaxis pathway to concerted variations in the expression levels of the chemotaxis proteins [66].

To extend these results to the case of time-varying activation rates that is more di-

rectly relevant to a situation in which the concentrations of the KaiC phosphoforms rise and fall, we allow $k_K(t)$ and $k_P(t)$ to vary with time as shown in Fig. 2.H.1C (upper graph): Similarly to the total KaiC concentration at $T_d = 48$ hours with $N = 1$ (Fig. 2.4C of the main text), each rate changes periodically with a period of 48 hours, with alternating higher and lower peaks. The lower graph of Fig. 2.H.1C , with time traces of $[S_p]$, $[K^*]$ and $[P^*]$, shows that even though the amplitude of $[K^*](t)$ and $[P^*](t)$ varies between oscillation cycles, the amplitude of $S_p(t)$ is constant. Comparable behavior is expected as long as the rates associated with the enzymatic reactions are faster than the timescale of variation of $k_K(t)$ and $k_P(t)$. Provided this is the case, the push-pull system built around RpaA will allow the bacterium to take as its clock readout the phosphorylation fraction $p(t)$—which we have argued is robust to perturbations associated with the cell cycle—rather than the absolute concentration of KaiC or one of its phosphoforms.

2.I. MULTIPLE CHROMOSOMES REDUCE THE COUPLING BETWEEN CLOCK AND CELL CYCLE IN TTC-PPC AND NTFO MODELS (FIG. 2.I.1)

Fig. 2.5C of the main text shows the average peak-to-peak time and its standard deviation for the TTC-($PPC_{Zwicker}$) model [19], as a function of the cell-division time T_d, both for $N = 1$ and for $N = 4$. Panel A of Fig. 2.I.1 shows exactly the same figure, but with underneath it, for $N = 4$, time traces for $p(t)$ and $C_{tot}(t)$ at $T_d = 24.5$ h (panel B) and $T_d = 48$ h (panel C), as also indicated by the arrows in panel A. As discussed in the main text, the effects of the cell cycle have almost completely disappeared, even at $T_d = 24.5$ h, immediately outside the locking regime, where the effects are usually most visible.

Panels D–G of Fig. 2.I.1 show the effect of multiple chromosomes on the locking behavior of the NTFO model. Panel D shows that with $N = 4$ chromosome copies at the beginning of the cell cycle, both the variance and the width of the locking regions have decreased to no more than one hour. The time traces (Fig. 2.I.1E–G) of the protein concentration at cell division times of 24, 27 and 48 hours confirm that the NTFO has indeed become very stable. At $T_d = 27$ hours, where the protein concentration had showed irregular behavior and large amplitude variations for $N = 1$, its behavior has now become much more regular. At a division time of 48 hours, the marked amplitude variations present when $N = 1$ have disappeared. Indeed, the beneficial effect of a higher gene-copy number is larger than that of adding a PPC, as can be seen by comparing Fig. 2.I.1D with Fig. 2.4 of the main text. Fig. 2.J.1 shows that essentially the same effect is also found in the TTC-($PPC_{Zwicker}$) model. Of course, the most stable clock is obtained when a higher gene copy number is combined with a PPC (see Fig. 2.5), suggesting that both are needed for circadian rhythms that are maximally resilient against perturbations from the cell cycle.

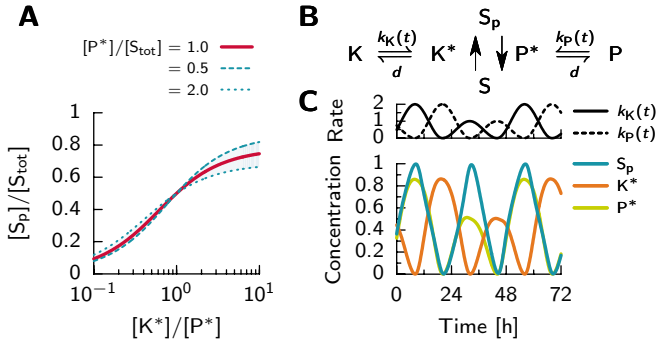

Figure 2.H.1: A push-pull network can read out the phosphorylation fraction $p(t)$ while remaining insensitive to the total concentration $C_{\mathrm{tot}}(t)$ of KaiC. (A) Steady-state output of the push-pull network, the fraction of phosphorylated substrate $[S_p]/[S_{tot}]$, plotted against the ratio of the active kinase concentration, $[K^*]$, to the active phosphatase concentration $[P^*]$; here, $[S_p]/[S_{tot}]$ mimics the phosphorylation fraction of RpaA. In steady state (but not necessarily in the general, time-varying case, see panel B) $[K^*]$ directly reports the concentration of KaiC in the phosphorylation phase of the clock and $[P^*]$ the concentration of KaiC in the clock's dephosphorylation phase. For the solid red line, we change $[K^*]/[P^*]$ from 0.1 to 10, while keeping $[P^*]$ equal to $[S_{tot}]$. The dashed and dotted lines show the result when both the kinase and phosphatase concentrations are halved or doubled, respectively. Because of the push-pull architecture, a change in the total concentration $[K^*]+[P^*]$ at fixed $[K^*]/[P^*]$ has only a small effect on the steady-state level of phosphorylated substrate $[S_p]/[S_{tot}]$; the network predominantly responds to the ratio $[K^*]/[P^*]$. (B) Schematic of our model of a simple push-pull network. The amount of active kinase, $[K^*]$, is controlled by the time-dependent rate $k_K(t)$ of conversion from K to K*, and similarly for $[P^*]$ and $k_P(t)$; we imagine that these rates are proportional to the amount of KaiC in the phosphorylation and dephosphorylation phases of the clock, respectively. The two enzymes return to their inactive states at constant rates d. The interconversion between S and S_p follows the standard Michaelis-Menten reaction scheme. (C) Reading out time-varying rates k_K and k_P. (Top) We let $k_K(t)$ oscillate with a peak-to-peak time of 24 hours, with the amplitude of each consecutive oscillation cycle changing by a factor of two to mimic the variability in the total amount of KaiC when $T_d = 48$ h (Fig. 2.2 of the main text). $k_P(t)$ has the same behavior as $k_K(t)$, but phase shifted by 12 hours. (Bottom) With these time-varying inputs, the active enzyme concentrations $[K^*]$ and $[P^*]$ track the conversion rates $k_K(t)$ and $k_P(t)$, but $[S_p]$ shows an essentially constant amplitude from one cycle to the next. Thus, even with time-varying inputs, the activity of RpaA is sensitive primarily to the ratio $k_K(t)/k_P(t)$, which plays the role of the phosphoryation ratio $p(t)$, not to each rate individually, or by extention to the absolute concentrations of KaiC phosphoforms. In all calculations, $K_M = [S_{tot}]$.

2.J. PHASE DIAGRAMS FOR THE NTFO, TTC-($PPC_{Zwicker}$) AND TTC-(PPC_{Rust}) MODELS (FIG. 2.J.1)

In order to get a better understanding of how the cell cycle perturbs the clock, we have made phase diagrams for both the width of the 1:1 locking region and the average variance of the peak-to-peak times, as a function of the two key variables that affect locking, the number of gene copies N and the standard deviation in their replication times, σ_{rep}, for all models, *i.e.* the NTFO model, the TTC-($PPC_{Zwicker}$) model of Zwicker *et al.* [19]

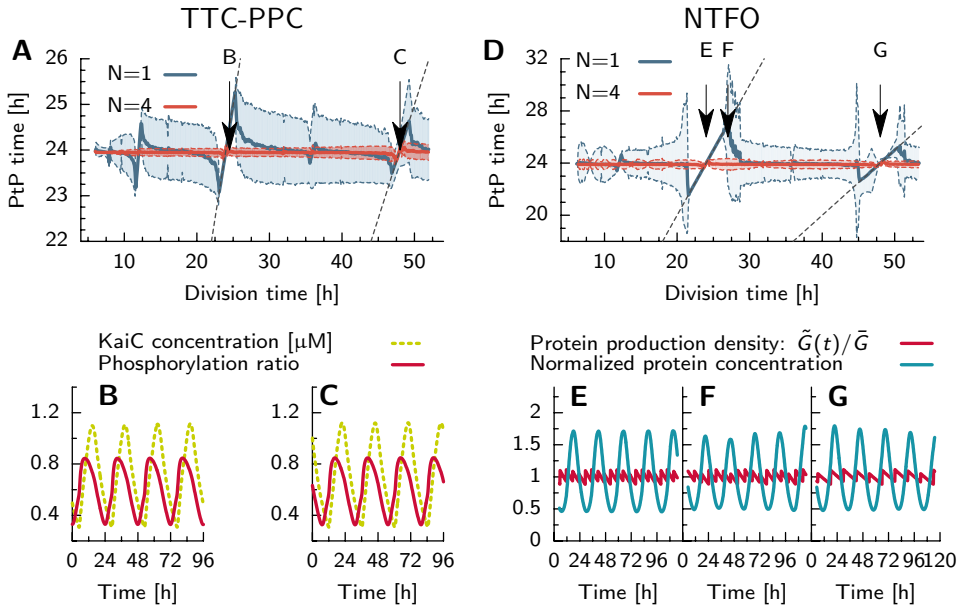

Figure 2.I.1: Multiple chromosome copies reduce the effect of periodic gene replications in both the TTC-($\text{PPC}_{\text{Zwicker}}$) model [19] (panels A–C) and in the simple negative transcriptional feedback oscillator (NTFO) (panels D–G). Panel (A) shows for the TTC-PPC model the average peak-to-peak time as a function of the cell-division time T_d for initial gene copy numbers $N = 1$ (blue) and $N = 4$ (red). This panel is identical to Fig. 2.5C of the main text, except for the arrows indicating the values of T_d for which times traces are shown in (B,C) for $N = 4$. Both the standard deviation in the peak-to-peak times (given by the shaded regions) and the regions where the oscillator is locked to the cell cycle are strongly reduced for $N = 4$. (B) The total KaiC concentration $C_{tot}(t)$ (dashed line) and phosphorylation fraction $p(t)$ (solid line) for the TTC-PPC model at $T_d = 24.5$ h, for $N = 4$. (C) $C_{tot}(t)$ and $p(t)$ at $T_d = 48$ h for the same model, again for $N = 4$. Note that, even at $T_d = 24.5$ h, immediately outside the locking region where the variance in T_{PtP} is generally largest, the effects of the cell cycle have almost completely disappeared. (D) The average peak-to-peak time and its standard deviation for the NTFO model, for $N = 1$ (blue line) and $N = 4$ (red line). It is seen that as in the Zwicker model, multiple chromosome copies dramatically reduce the strength of locking. (E–G) NTFO time traces of the protein-concentration oscillations $C(t)$ (blue lines) and the production density $\tilde{G}(t)$ (red lines), both normalized to their time average values, for $N = 4$, and for cell-division times indicated by the arrows in (D). With $N = 4$, only at, or very close to $T_d = 24$ hr (E), is the NTFO locked to the cell cycle. Even at $T_d = 27$ h (F) and $T_d = 48$ h (G), where for $N = 1$ the NTFO shows irregular behavior and large amplitude variations, respectively (see Fig. 2.2C,D), the time courses are much less perturbed by the cell cycle when $N = 4$. However, albeit greatly reduced, the effect of driving by the cell cycle can nonetheless still be observed, both in the persistence of small regions of locking and in the still appreciable variance in T_{PtP} when the oscillators are not locked (panel D). A PPC must be added to more fully attenuate the cell cycle's influence. (Compare panel D with panel A, taking into account the difference in scale of the y-axis; the standard deviation of T_{PtP} is about 3 times larger for the NTFO than for the full TTC-PPC model.)

and the TTC-(PPC$_{\text{Rust}}$) model [19, 22].

To make phase diagrams as a function N and σ_{rep}, we need to extend our model of stochasticity in the timing of gene replication introduced earlier in this document for $N = 1$, to also allow for a higher gene copy number, $N > 1$. Each cell cycle has N gene replication events which occur at times t_{g}^i within the interval $[0, T_{\text{d}})$. Each replication time is drawn from a Gaussian distribution with a standard deviation σ_{rep} that is proportional to T_{d}, and a mean $\bar{t}_{\text{g}}^i = T_{\text{d}}/N(\frac{1}{2} + i)$, where $i \in \{0, \ldots, N-1\}$ for each cell cycle. Replication times $t_{\text{g}}'^i$ that fall outside the interval $[0, T_{\text{d}})$, are mapped back onto it via $t_{\text{g}}^i = \text{Mod}(t_{\text{g}}'^i, T_{\text{d}})$. Note that this mapping slightly decreases the variance in the replication times; the real variance will therefore be slightly less than σ_{rep}^2 (at most 10%).

We run simulations with values for $\sigma_{\text{rep}}/T_{\text{d}}$ in the range $[0, 0.3]$, which, as mentioned above, corresponds to a scenario where the replication time is essentially chosen at random between 0 and T_{d}. We consider initial gene copy numbers of $N \in \{1, 2, 3, 4\}$.

Panels A, E, and I of Fig. 2.J.1 show the phase diagrams of the width of the 1:1 locking regions as a function of N and $\sigma_{\text{rep}}/T_{\text{d}}$, for the NTFO, TTC-(PPC$_{\text{Zwicker}}$) and TTC-(PPC$_{\text{Rust}}$) models, respectively. The panels underneath, (B, F, J), respectively, show cuts through these phase diagrams. Here, we consider an oscillator to be 1:1 locked to the cell cycle when the difference between its average PtP-time, $\langle T_{\text{PtP}} \rangle$, and the cell-division time T_{d} is less than 0.05 hour: $\langle T_{\text{PtP}}(T_{\text{d}}) \rangle - T_{\text{d}} < 0.05$.

Panels C, G, K of Fig. 2.J.1 show the phase diagrams of the average variance in the peak-to-peak times, $\langle \sigma_{\text{PtP}}^2 \rangle$, again as a function of N and $\sigma_{\text{rep}}/T_{\text{d}}$, for the NTFO, TTC-(PPC$_{\text{Zwicker}}$) and TTC-(PPC$_{\text{Rust}}$) models, respectively. Here, the variance is averaged over a range of cell-division times $6 < T_{\text{d}} < 52$:

$$\langle \sigma_{\text{PtP}}^2 \rangle = \frac{1}{N_{\text{sim}}} \sum_{i=1}^{N_{\text{sim}}} \sigma_{\text{PtP}}^2(T_{\text{d}}^i), \tag{2.20}$$

where N_{sim} is the number of evenly-spaced simulations performed in the range $6 < T_{\text{d}} < 52$ in steps of 0.1 hour, and $\sigma_{\text{PtP}}^2(T_{\text{d}}^i)$ is the variance in the PtP-times for 5000 hours of simulated time at cell-divistion time T_{d}^i. This quantity is a measure for the erratic behavior induced by the coupling to the cell cycle outside the locking region.

It seen that for all models both the width of the 1:1 locking region (Fig. 2.J.1, panels A/B, E/F, I/J) and the variance in the peak-to-peak times (Fig. 2.J.1, panels C/D, G/H, K/L), initially rapidly decreases with N, but then reaches a plateau. Even in the limit that $N \to \infty$, there is still some weak, residual driving by the cell cycle, because N rises linearly while the volume V rises exponentially during the cell cycle, leading to periodic variations in the gene density $G(t) = N(t)/V(t)$. It is also seen that the width of the 1:1 locking region decreases with increasing σ_{rep}, especially when N is small. However, while increasing the noise in the timing of replication reduces the width of the locking region, it also strongly increases the variance in the peak-to-peak times. A reliable clock requires not only a small locking window, but also a small peak-to-peak variance. Clearly, allowing for stochasticity in the timing of replication is not a solution to the locking problem.

Comparing the different models, it is seen that building the clock around a PPC reduces not only the width of the locking region, but also the variance in the peak-to-peak times, both in the TTC-(PPC$_{\text{Zwicker}}$) (Fig. 2.J.1E–H) and in the TTC-(PPC$_{\text{Rust}}$) model

(Fig. 2.J.1I–L). However, with $N = 1$ chromosome copy at the beginning of the cell cycle, the introduction of the PPC is not sufficient to fully eliminate locking. A TTC-PPC model still requires multiple chromosome copies that are replicated asynchronously.

2.K. METHODS

The delay-differential equations (DDE) describing our models in the absence of noise were propagated using the numerical differential equation solver of Mathematica 8 (Wolfram Research). For each value of T_d, we generated a single time trace of 2000 hours. In order to allow the oscillations to settle down to a steady state, we discarded the first 500 hours of each simulation and analyzed the remaining 1500 hours.

To find the peak-to-peak times T_{PtP} in the deterministic DDE simulations (including those with noise in the gene replication times), we used the built-in methods of Mathematica to return all local extrema in the concentration and phosphorylation fraction, respectively; these extrema correspond to the time points t_i where C_i or, respectively, p_i, is higher, in the case of a maximum, or lower, in the case of a minimum, than its two immediate neighbors. As is standard for numerical solution of differential equations, the spacing $t_i - t_{i-1}$ between successive time points was determined adaptively by the algorithm to meet imposed precision bounds but never exceeded 0.2 h. We then checked if a given local minimum was the lowest point within an interval of ± 18 hours centered on the minimum; if so, we defined this point as the global minimum of a single oscillation cycle. If there did exist a local extremum with a lower value, we repeated this procedure around the lower point until we found a point which was the lowest within a time interval of ± 18 hours. The same procedure was followed for the local maxima. The peak-to-peak time was then calculated by subtracting the times of two consecutive minima; we verified that substracting the times of two consecutive *maxima* gave essentially the same results.

To find the peak to peak times in the kinetic Monte Carlo simulation of the NTFO, we record the protein concentration $c_i(t_i)$ every 0.01 h of simulated time. We then use a sliding window of 18 hours over these concentrations to find the extrema of the oscillations. Specifically, to find the time t_j of the next local minimum: starting from the maximum of the preceding oscillation cycle at time t_i, we find the smallest concentration c_j, with $j > i$, in the window $t_j - t_i \leq 18$ h. (Given c_i was a local maxmium, there must exist a concentration $c_j < c_i$.) We then check whether there exists a concentration $c_k < c_j$ for $k > j$ and $t_k - t_j \leq 18$ h. If there is, we replace c_j by c_k and again search for a deeper minimum within 18 hours; otherwise, c_j is the minimum of the next oscillation cycle. A completely analogous procedure is used to identify the maxima of successive oscillation cycles.

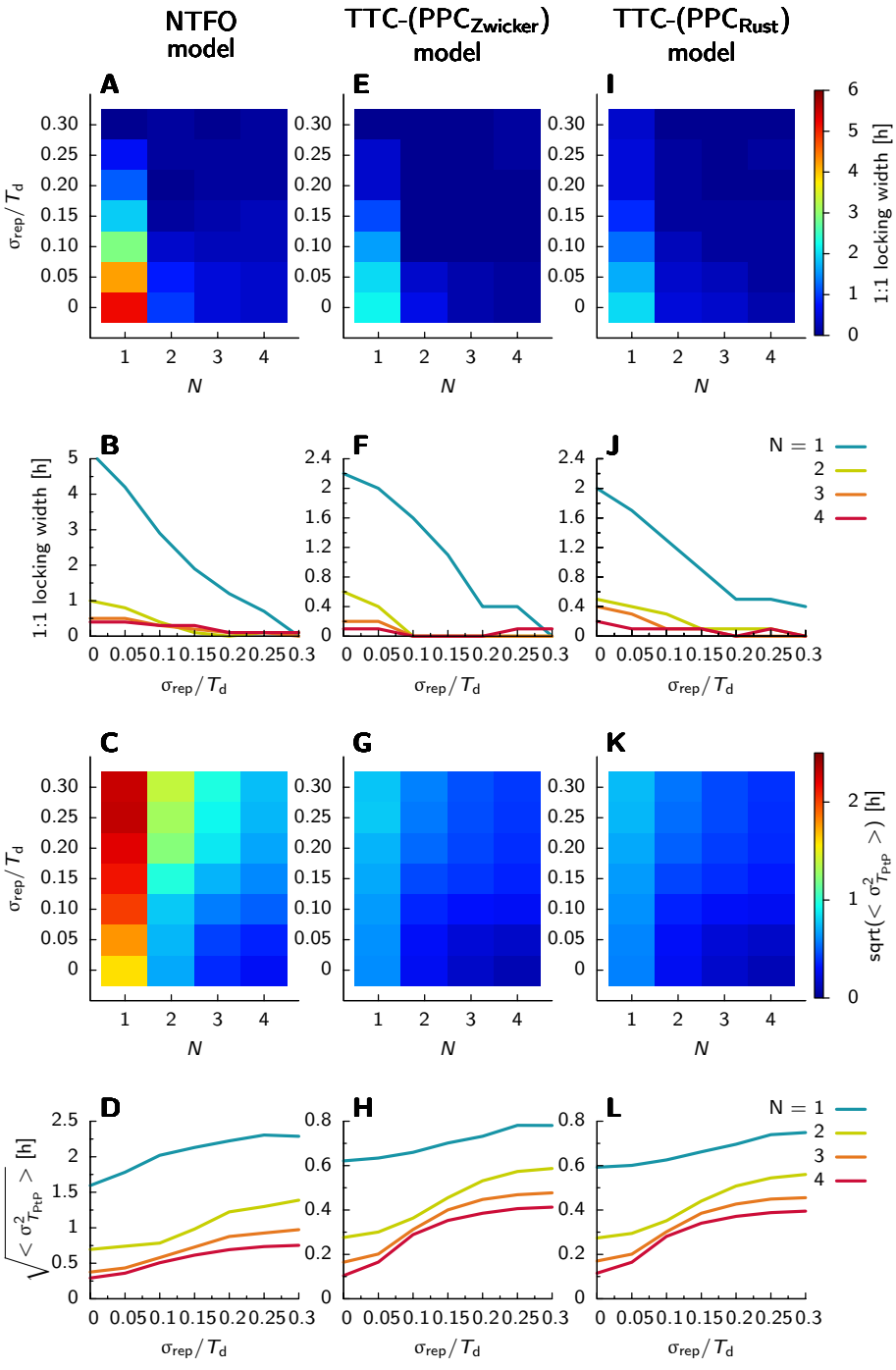
NTFO model
TTC-(PPC$_{Zwicker}$) model
TTC-(PPC$_{Rust}$) model
A
E
I
B
F
J
C
G
K
D
H
L
σ_{rep}/T_d
N
1:1 locking width [h]
N = 1
2
3
4
sqrt($<\sigma^2_{T_{PtP}}>$) [h]
$\sqrt{<\sigma^2_{T_{PtP}}>}$ [h]

Figure 2.J.1 ***(preceding page):*** Heat plots of the width of the 1:1 locking region (panels, A, E, I) and the average standard deviation of the peak-to-peak time (panels C, G, K), as a function of the initial gene copy number N and the standard deviation in the gene replication time $\sigma_{\mathrm{rep}}/T_{\mathrm{d}}$, for the NTFO model (panels A–D), the TTC-(PPC$_{\mathrm{Zwicker}}$) model [19] (panels E–H), and the TTC-(PPC$_{\mathrm{Rust}}$) model [19, 22] (panel I–L). Panels B,D,F,H,J,L show the same data as in the heat plots immediately above them, but as a function of $\sigma_{\mathrm{rep}}/T_{\mathrm{d}}$, for different values of N; *note the difference in scale of the y-axes* in these panels. The major results of panels B, D, F, and H are also summarized in Fig. 2.5C, D of the main text. The average standard deviation in the peak-to-peak time is the standard deviation in the peak-to-peak time averaged over $6 < T_{\mathrm{d}} < 52$; it is a measure for the erratic behavior of the clock outside the locking regions. It is seen that in all models the width of the locking region rapidly decreases with both N and $\sigma_{\mathrm{rep}}/T_{\mathrm{d}}$. However, the average standard deviation in the peak-to-peak time decreases with N, but increases with $\sigma_{\mathrm{rep}}/T_{\mathrm{d}}$. Clearly, while having multiple chromosome copies is a powerful strategy for preventing locking, increasing the stochasticity in the timing of gene replication is not—decreasing locking at the expense of much greater variation in the length of the periodic is unlikely to be functionally advantageous. Comparing the two models with a PPC to the NTFO model shows that adding a PPC to a TTC also decreases both the width of the locking region and the average standard deviation in the peak-to-peak time. Combining both features—a PPC and multiple chromosome copies—gives the strongest reduction in the coupling of the clock to the cell cycle.

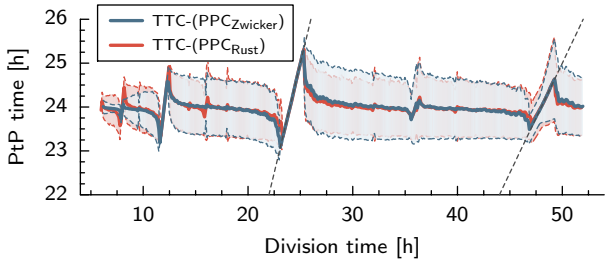

Figure 2.K.1: The TTC-(PPC$_{\mathrm{Rust}}$) model, which combines the TTC of Zwicker *et al.* with the PPC of Rust and coworkers [22], is susceptible to periodic gene replication. The figure shows the average and standard deviation of the peak-to-peak time T_{PtP} of the phosphorylation fraction $p(t)$ for the TTC-(PPC$_{\mathrm{Rust}}$) model and the TTC-(PPC$_{\mathrm{Zwicker}}$) model [19]. Clearly, the two models are similarly affected by the presence of the cell cycle.

BIBLIOGRAPHY

[1] Johnson CH, Egli M, Stewart PL (2008) Structural insights into a circadian oscillator. *Science* 322:697–701.

[2] Elowitz MB, Levine AJ, Siggia ED (2002) Stochastic gene expression in a single cell. *Science* 297:1183–1186.

[3] Mori T, Binder B, Johnson CH (1996) Circadian gating of cell division in cyanobacteria growing with average doubling times of less than 24 hours. *Proc Natl Acad Sci* 93:10183–10188.

[4] Walker N, Nghe P, Tans SJ (2016) Generation and filtering of gene expression noise by the bacterial cell cycle. *BMC Biol* 14:11.

[5] Kondo T, et al. (1993) Circadian rhythms in prokaryotes : Luciferase as a reporter of circadian gene expression in cyanobacteria. *Proc Natl Acad Sci* 90:5672–5676.

[6] Pfeuty B, Thommen Q, Lefranc M (2011) Robust entrainment of circadian oscillators requires specific phase response curves. *Biophys J* 100:2557–2565.

[7] Rust MJ, Golden SS, O'Shea EK (2011) Light-driven changes in energy metabolism directly entrain the cyanobacterial circadian oscillator. *Science* 331:220–223.

[8] DeMairan J (1729) *Histoire de l'Academie Royale des Sciences* (Academie Royale des Sciences, Paris), pp 35–36.

[9] Konopka RJ, Benzer S (1971) Clock mutants of Drosophila melanogaster. *Proc Natl Acad Sci* 68:2112–2116.

[10] Ishiura M, et al. (1998) Expression of a gene cluster kaiABC as a circadian feedback process in cyanobacteria. *Science* 281:1519–1523.

[11] Nishiwaki T, et al. (2004) Role of KaiC phosphorylation in the circadian clock system of Synechococcus elongatus PCC 7942. *Proc Natl Acad Sci* 101:13927–13932.

[12] Nakajima M, et al. (2005) Reconstitution of circadian oscillation of cyanobacterial KaiC phosphorylation in vitro. *Science* 308:414–415.

[13] Bialek W (2015) Perspectives at the interface of physics and biology. *arXiv* 1512.08954.

[14] Emberly E, Wingreen NS (2006) Hourglass model for a protein-based circadian oscillator. *Phys Rev Lett* 96:038303.

[15] van Zon JS, Lubensky DK, Altena PRH, ten Wolde PR (2007) An allosteric model of circadian KaiC phosphorylation. *Proc Natl Acad Sci* 104:7420–7425.

[16] Eguchi K, Yoda M, Terada TP, Sasai M (2008) Mechanism of robust circadian oscillation of KaiC phosphorylation in vitro. *Biophys J* 95:1773–1784.

[17] Yoda M, Eguchi K, Terada TP, Sasai M (2007) Monomer-shuffling and allosteric transition in KaiC circadian oscillation. *PLoS One* 5:1–8.

[18] Lin J, Chew J, Chockanathan U, Rust MJ (2014) Mixtures of opposing phosphorylations within hexamers precisely time feedback in the cyanobacterial circadian clock. *Proc Natl Acad Sci* 111:E3937–E3945.

[19] Zwicker D, Lubensky DK, ten Wolde PR (2010) Robust circadian clocks from coupled protein- modification and transcription-translation cycles. *Proc Natl Acad Sci* 107:22540–22545.

[20] Teng SW, Mukherji S, Moffitt JR, de Buyl S, O'Shea EK (2013) Robust circadian oscillations in growing cyanobacteria require transcriptional feedback. *Science* 340:737–740.

[21] Paijmans J, Bosman M, ten Wolde PR, Lubensky DK (2016) Discrete gene replication events drive coupling between the cell cycle and circadian clocks. *Proc Natl Acad Sci* 113:4063–4068.

[22] Rust MJ, Markson JS, Lane WS, Fisher DS, O'Shea EK (2007) Ordered phosphorylation governs oscillation of a three-protein circadian clock. *Science* 318:809–812.

[23] Tsai TYC, et al. (2008) Robust, tunable biological oscillations from interlinked positive and negative feedback loops. *Science* 321:126–129.

[24] Li C, Chen X, Wang P, Wang W (2009) Circadian KaiC phosphorylation : A multi-Layer network. *PLoS Comput Biol* 5:e1000568.

[25] Nagai T, Terada TP, Sasai M (2010) Synchronization of circadian oscillation of phosphorylation level of KaiC in vitro. *Biophys J* 98:2469–2477.

[26] Phong C, Markson JS, Wilhoite CM, Rust MJ (2013) Robust and tunable circadian rhythms from differentially sensitive catalytic domains. *Proc Natl Acad Sci* 110:1124–1129.

[27] Chang Yg, et al. (2015) A protein fold switch joins the circadian oscillator to clock output in cyanobacteria. *Science* 349:324–328.

[28] Elowitz MB, Leibler S (2000) A synthetic oscillatory network of transcriptional regulators. *Nature* 403:335–338.

[29] Stricker J, et al. (2008) A fast, robust and tunable synthetic gene oscillator. *Nature* 456:516–520.

[30] Pattanayak GK, Lambert G, Bernat K, Rust MJ (2015) Controlling the cyanobacterial clock by synthetically rewiring metabolism. *Cell Rep* 13:2362–2367.

[31] Salter MG, Franklin KA, Whitelam GC (2003) Gating of the rapid shade-avoidance response by the circadian clock in plants. *Nature* 426:680–683.

[32] Johnson C (2010) Circadian clocks and cell division: What's the pacemaker? *Cell Cycle* 9:3864–3873.

[33] Sotak M, Sumova A, Pacha J (2014) Cross-talk between the circadian clock and the cell cycle in cancer. *Ann Med* 46:221–232.

[34] Matsuo T, et al. (2003) Control mechanism of the circadian clock for timing of cell division in vivo. *Science* 302:255–259N.

[35] Nagoshi E, et al. (2004) Circadian gene expression in individual fibroblasts: Cell-autonomous and self-sustained oscillators pass time to daughter cells. *Cell* 119:693–705.

[36] Dong G, et al. (2010) Elevated ATPase activity of KaiC applies a circadian checkpoint on cell division in Synechococcus elongatus. *Cell* 140:529–539.

[37] Yang Q, Pando BF, Dong G, Golden SS, van Oudenaarden A (2010) Circadian gating of the cell cycle revealed in single cyanobacterial cells. *Science* 327:1522–1526.

[38] Gerard C, Goldbeter A (2012) Entrainment of the mammalian cell cycle by the circadian clock: Modeling two coupled cellular rhythms. *PLoS Comp Biol* 8:e1002516.

[39] Feillet C, et al. (2014) Phase locking and multiple oscillating attractors for the coupled mammalian clock and cell cycle. *Proc Natl Acad Sci* 111:9828–9833.

[40] Bieler J, et al. (2014) Robust synchronization of coupled circadian and cell cycle oscillators in single mammalian cells. *Mol Syst Biol* 10:739.

[41] Bosman M (2012) Master's thesis (Universiteit van Amsterdam).

[42] Volfson D, et al. (2006) Origins of extrinsic variability in eukaryotic gene expression. *Nature* 439:861–864.

[43] Irish VF, Gelbart WM (1987) The decapentaplegic gene is required for dorsal-ventral patterning of the Drosophila embryo. *Genes Dev* 1:868–879.

[44] Trcek T, Larson DR, Moldon A, Query CC, Singer RH (2011) Single-molecule mRNA decay measurements reveal promoter-regulated mRNA stability in yeast. *Cell* 147:1484–1497.

[45] Zopf CJ, Quinn K, Zeidman J, Maheshri N (2013) Cell-Cycle dependence of transcription dominates noise in gene expression. *PLoS Comp Biol* 9:e1003161.

[46] Narula J, et al. (2015) Chromosomal arrangement of phosphorelay genes couples sporulation and DNA replication. *Cell* 162:328–337.

[47] Hensel Z, Marquez-Lago TT (2015) Cell-cycle-synchronized, oscillatory expression of a negatively autoregulated gene in E. coli. *arXiv* 1506.08596.

[48] Pikovsky A, Rosenblum M, Kurths J (2003) *Synchronisation: A universal concept in nonlinear sciences* (Cambridge University Press, Cambridge).

[49] Mori T, Johnson CH (2001) Independence of circadian timing from cell division in cyanobacteria. *J. Bacteriol.* 183:2439–2444.

[50] Kageyama H, et al. (2006) Cyanobacterial circadian pacemaker: Kai protein complex dynamics in the KaiC phosphorylation cycle in vitro. *Mol Cell* 23:161–171.

[51] Clodong S, et al. (2007) Functioning and robustness of a bacterial circadian clock. *Mol Syst Biol* 3:90.

[52] Brettschneider C, et al. (2010) A sequestration feedback determines dynamics and temperature entrainment of the KaiABC circadian clock. *Mol Syst Biol* 6:1–10.

[53] Qin X, Byrne M, Xu Y, Mori T, Johnson CH (2010) Coupling of a core post-translational pacemaker to a slave transcription/translation feedback loop in a circadian system. *PLoS Biol* 8:e1000394.

[54] Takai N, et al. (2006) A KaiC-associating SasA-RpaA two-component regulatory system as a major circadian timing mediator in cyanobacteria. *Proc Natl Acad Sci* 103:12109–12114.

[55] Taniguchi Y, Takai N, Katayama M, Kondo T, Oyama T (2010) Three major output pathways from the KaiABC-based oscillator cooperate to generate robust circadian kaiBC expression in cyanobacteria. *Proc Natl Acad Sci* 107:3263–3268.

[56] Gutu A, O'Shea EK (2013) Two antagonistic clock-regulated histidine kinases time the activation of circadian gene expression. *Mol Cell* 50:288–294.

[57] Markson JS, Piechura JR, Puszynska AM, O'Shea EK (2013) Circadian control of global gene expression by the cyanobacterial master regulator RpaA. *Cell* 155:1396–1408.

[58] Jain IH, Vijayan V, O'Shea EK (2012) Spatial ordering of chromosomes enhances the fidelity of chromosome partitioning in cyanobacteria. *Proc Natl Acad Sci* 109:13638–13643.

[59] Lengeler JW, Drews G, Schlegel HG (1999) *Biology of the Prokaryotes* (Georg Thieme Verlag), p 481.

[60] Nishiwaki T, et al. (2007) A sequential program of dual phosphorylation of KaiC as a basis for circadian rhythm in cyanobacteria. *EMBO J* 26:4029–4037.

[61] Goldbeter A, Koshland DE (1981) An amplified sensitivity arising from covalent modification in biological systems. *Proc Natl Acad Sci* 78:6840–6844.

[62] Binder BJ, Chisholm SW (1990) Relationship between DNA cycle and growth rate in Synechococcus sp. strain PCC 6301. *J Bact* 172:2313–2319.

[63] Griese M, Lange C, Soppa J (2011) Ploidy in cyanobacteria. *FEMS Micr Lett* 323:124–131.

[64] Chen AH, Afonso B, Silver Pa, Savage DF (2012) Spatial and temporal organization of chromosome duplication and segregation in the cyanobacterium Synechococcus elongatus PCC 7942. *PLoS ONE* 7:e47837.

[65] Watanabe S, et al. (2012) Light-dependent and asynchronous replication of cyanobacterial multi-copy chromosomes. *Mol Microbiol* 83:856–865.

[66] Kollmann M, Løvdok L, Bartholomé K, Timmer J, Sourjik V (2005) Design principles of a bacterial signalling network. *Nature* 438:504–507.

[67] Shultzaberger RK, Boyd JS, Katsuki T, Golden SS, Greenspan RJ (2014) Single mutations in sasA enable a simpler ΔcikA gene network architecture with equivalent circadian properties. *Proc Natl Acad Sci* 111:E5069–E5075.

[68] Masri S, Cervantes M, Sassone-Corsi P (2013) The circadian clock and cell cycle: Interconnected biological circuits. *Curr Opin Cell Biol* 25:730–734.

[69] Ito H, et al. (2009) Cyanobacterial daily life with Kai-based circadian and diurnal genome-wide transcriptional control in Synechococcus elongatus. *Proc Natl Acad Sci* 106:14168–14173.

[70] Tomita J, Nakajima M, Kondo T, Iwasaki H (2005) No transcription-translation feedback in circadian rhythm of KaiC phosphorylation. *Science* 307:251–254.

[71] Delaune EA, Francois P, Shih NP, Amacher SL (2012) Single-cell-resolution imaging of the impact of Notch signaling and mitosis on segmentation clock dynamics. *Dev Cell* 23:995–1005.

[72] Bird AJ, Turner-Cavet JS, Lakey JH, Robinson NJ (1998) A carboxyl-terminal Cys2/His2-type zinc-finger motif in DNA primase influences DNA content in Synechococcus PCC 7942. *J Biol Chem* 273:21246–52.

[73] Kitayama Y, Nishiwaki T, Terauchi K, Kondo T (2008) Dual KaiC-based oscillations constitute the circadian system of cyanobacteria. *Genes Dev* 22:1513–1521.

[74] Collins JJ, Gardner TS, Cantor CR (2000) Construction of a genetic toggle switch in Escherichia coli. *Nature* 403:339–342.

[75] Becskei a, Serrano L (2000) Engineering stability in gene networks by autoregulation. *Nature* 405:590–593.

[76] Ernesto A, Basu S, Karig DK, Weiss R (2006) Synthetic biology: New engineering rules for an emerging discipline. *Mol Syst Biol* 2:1–14.

[77] Tigges M, Marquez-Lago TT, Stelling J, Fussenegger M (2009) A tunable synthetic mammalian oscillator. *Nature* 457:309–312.

[78] Nandagopal N, Elowitz MB (2011) Synthetic Biology: Integrated Gene Circuits. *Science* 333:1244–1248.

[79] Sowa SW, Gelderman G, Contreras LM (2015) Advances in synthetic dynamic circuits design: Using novel synthetic parts to engineer new generations of gene oscillations. *Curr Opin Biotechnol* 36:161–167.

[80] Elowitz MB, Hsing W, Leibler S (2002) Combinatorial synthesis of genetic networks. *Science* 296:1466–1470.

[81] Rosenfeld N, Young JW, Alon U, Swain PS, Elowitz MB (2005) Gene regulation at the single-cell level. *Science* 307:1962–1965.

[82] Cai L, Friedman N, Xie XS (2006) Stochastic protein expression in individual cells at the single molecule level. *Nature* 440:358–362.

[83] Chabot JR, Pedraza JM, Luitel P, van Oudenaarden A (2007) Stochastic gene expression out-of-steady-state in the cyanobacterial circadian clock. *Nature* 450:1249–1252.

[84] Novak B, Tyson JJ (2008) Design principles of biochemical oscillators. *Nat Rev Mol Cell Biol* 9:981–991.

[85] Mather W, Bennett MR, Hasty J, Tsimring LS (2009) Delay-induced degrade-and-fire oscillations in small genetic circuits. *Phys Rev Lett* 068105:1–4.

[86] Woods ML, Leon M, Perez-Carrasco R, Barnes CP (2016) A statistical approach reveals designs for the most robust stochastic gene oscillators. *ACS Synth Biol* 5:459–470.

[87] Garcia-Ojalvo J, Elowitz MB, Strogatz SH (2004) Modeling a synthetic multicellular clock: repressilators coupled by quorum sensing. *Proc Natl Acad Sci* 101:10955–10960.

[88] Mondragón-Palomino O, Danino T, Selimkhanov J, Tsimring L, Hasty J (2011) Entrainment of a population of synthetic genetic oscillators. *Science* 333:1315–1319.

[89] Prindle A, et al. (2014) Rapid and tunable post-translational coupling of genetic circuits. *Nature* 508:387–391.

[90] Kang B, Li YY, Chang X, Liu L, Li YX (2008) Modeling the effects of cell cycle M-phase transcriptional inhibition on circadian oscillation. *PLoS Comput Biol* 4:e1000019.

[91] Gonze D (2013) Modeling the effect of cell division on genetic oscillators. *J Theor Biol* 325:22–33.

[92] Dies M, Galera-Laporta L, Garcia-Ojalvo J (2015) Mutual regulation causes co-entrainment between a synthetic oscillator and the bacterial cell cycle. *Integr Biol*.

[93] Cooper S, Helmstetter CE (1968) Chromosome replication and the division cycle of Escherichia coli Br. *J Mol Biol* 31:519–540.

[94] Donachie W (1968) Relationship between cell size and time of initiation of DNA replication. *Nature* 219:1077–1079.

[95] Wallden M, Fange D, Gregorsson Lundius E, Baltekin Ö, Elf J (2016) The synchronization of replication and division cycles in individual E. coli cells. *Cell* 166:729–739.

[96] Adiciptaningrum A, Osella M, Moolman MC, Cosentino Lagomarsino M, Tans SJ (2015) Stochasticity and homeostasis in the E. coli replication and division cycle. *Sci Rep* 5:18261.

[97] Koppes LJH, Meyer M, Oonk HB, de Jong MA, Nanninga N (1980) Correlation between size and age at different events in the cell division cycle of Escherichia coli. *J Bacteriol* 143:1241–1252.

[98] Michelsen O, Teixeira de MJ, Jensen PR, Hansen FG (2003) Precise determinations of C and D periods by flow cytometry in Escherichia coli K-12 and B/r. *Microbiology* 149:1001–1010.

[99] Bogan JA, et al. (2001) P1 and NR1 plasmid replication during the cell cycle of Escherichia coli. *Plasmid* 45:200–208.

[100] Mori T, Johnson CH (2001) Independence of circadian timing from cell division in cyanobacteria independence of circadian timing from cell division in cyanobacteria. *J Bacteriol* 183:2439–2444.

[101] Hurley JM, Loros JJ, Dunlap JC (2016) Circadian oscillators: Around the transcription–translation feedback loop and on to output. *Trends Biochem Sci* 41:834–846.

[102] Xu Y, Mori T, Johnson CH (2000) Circadian clock-protein expression in cyanobacteria: Rhythms and phase setting. *EMBO J* 19:3349–3357.

[103] Nakahira Y, et al. (2004) Global gene repression by KaiC as a master process of prokaryotic circadian system. *Proc Natl Acad Sci* 101:881–885.

[104] Mehra A, et al. (2006) Circadian rhythmicity by autocatalysis. *PLoS Comput Biol* 2:1–8.

[105] Clodong S, et al. (2007) Functioning and robustness of a bacterial circadian clock. *Mol Syst Biol* 3:1–9.

[106] Mori T, et al. (2007) Elucidating the ticking of an in vitro circadian clockwork. *PLoS Biol* 5:0841–0853.

[107] Miyoshi, Fumihiko and Nakayama, Yoichi and Kaizu, Kazunari and Iwasaki, Hideo and Tomita M (2007) A mathematical model for the Kai-protein–based chemical oscillator and cock gene expression rhythms in cyanobacteria. *J Biol Rhythms* 22:69–80.

[108] Markson JS, O'Shea EK (2009) The molecular clockwork of a protein-based circadian oscillator. *FEBS Lett* 583:3938–3947.

[109] Williams S, Vakonakis I (2002) Structure and function from the circadian clock protein KaiA of Synechococcus elongatus: A potential clock input mechanism. *Proc Natl Acad Sci* 99:15357–15362.

[110] Iwasaki H, Nishiwaki T, Kitayama Y, Nakajima M, Kondo T (2002) KaiA-stimulated KaiC phosphorylation in circadian timing loops in cyanobacteria. *Proc Natl Acad Sci* 99:15788–15793.

[111] Xu Y, Mori T, Johnson CH (2003) Cyanobacterial circadian clockwork: roles of KaiA, KaiB and the kaiBC promoter in regulating KaiC. *EMBO J* 22:2117–2126.

[112] Kitayama Y, Iwasaki H, Nishiwaki T, Kondo T (2003) KaiB functions as an attenuator of KaiC phosphorylation in the cyanobacterial circadian clock system. *EMBO J* 22:2127–2134.

[113] Pattanayek R, et al. (2008) Structural model of the circadian clock KaiB-KaiC complex and mechanism for modulation of KaiC phosphorylation. *EMBO J* 27:1767–1778.

[114] Terauchi K, et al. (2007) ATPase activity of KaiC determines the basic timing for circadian clock of cyanobacteria. *Proc Natl Acad Sci* 104:16377–16381.

[115] Murakami R, et al. (2008) ATPase activity and its temperature compensation of the cyanobacterial clock protein KaiC. *Genes Cells* 13:387–95.

[116] Nishiwaki T, Kondo T (2012) Circadian autodephosphorylation of cyanobacterial clock protein KaiC occurs via formation of ATP as intermediate. *J Biol Chem* 287:18030–18035.

[117] Egli M, et al. (2012) Dephosphorylation of the core clock protein KaiC in the cyanobacterial KaiABC circadian oscillator proceeds via an ATP synthase mechanism. *Biochemistry* 51:1547–1558.

[118] Mori T, et al. (2002) Circadian clock protein KaiC forms ATP-dependent hexameric rings and binds DNA. *Proc Natl Acad Sci* 99:17203–17208.

[119] Hayashi F, Suzuki H, Iwase R (2003) ATP induced hexameric ring structure of the cyanobacterial circadian clock protein KaiC. *Genes to Cells* 8:287–296.

[120] Hayashi F, et al. (2004) Roles of two ATPase-motif-containing domains in cyanobacterial circadian clock protein KaiC. *J Biol Chem* 279:52331–52337.

[121] Nishiwaki T, Iwasaki H, Ishiura M, Kondo T (2000) Nucleotide binding and autophosphorylation of the clock protein KaiC as a circadian timing process of cyanobacteria. *Proc Natl Acad Sci* 97:495–499.

[122] Chang Yg, Tseng R, Kuo NW, Liwang A (2012) Rhythmic ring-ring stacking drives the circadian oscillator clockwise. *Proc Natl Acad Sci* 109:16847–16851.

[123] Kim YI, Dong G, Carruthers CW, Golden SS, LiWang A (2008) The day/night switch in KaiC, a central oscillator component of the circadian clock of cyanobacteria. *Proc Natl Acad Sci* 105:12825–12830.

[124] Chang Yg, Kuo Nw, Tseng R, Liwang A (2011) Flexibility of the C-terminal , or CII , ring of KaiC governs the rhythm of the circadian clock of cyanobacteria. *Proc Natl Acad Sci* 108:14431–14436.

[125] Egli M, et al. (2013) Loop-loop interactions regulate KaiA-stimulated KaiC phosphorylation in the cyanobacterial KaiABC circadian clock. *Biochemistry* 52:1208–1220.

[126] Snijder J, et al. (2014) Insight into cyanobacterial circadian timing from structural details of the KaiB-KaiC interaction. *Proc Natl Acad Sci* 111:1379–1384.

[127] Nishiwaki-Ohkawa T, Kitayama Y, Ochiai E, Kondo T (2014) Exchange of ADP with ATP in the CII ATPase domain promotes autophosphorylation of cyanobacterial clock protein KaiC. *Proc Natl Acad Sci* 111:4455–4460.

[128] Monod J, Wyman J, Changeux JP (1965) On the nature of allosteric transitions: A plausible model. *J Mol Biol* 12:88–118.

[129] Kageyama H, Kondo T, Iwasaki H (2003) Circadian formation of clock protein complexes by KaiA, KaiB, KaiC, and SasA in cyanobacteria. *J Biol Chem* 278:2388–2395.

[130] Nakajima M, Ito H, Kondo T (2010) In vitro regulation of circadian phosphorylation rhythm of cyanobacterial clock protein KaiC by KaiA and KaiB. *FEBS Lett* 584:898–902.

[131] Pattanayek R, et al. (2006) Analysis of KaiA-KaiC protein interactions in the cyanobacterial circadian clock using hybrid structural methods. *EMBO J* 25:2017–2028.

[132] Kitayama Y, Nishiwaki-Ohkawa T, Sugisawa Y, Kondo T (2013) KaiC intersubunit communication facilitates robustness of circadian rhythms in cyanobacteria. *Nat Commun* 4:2897.

[133] Hayashi F, et al. (2004) Stoichiometric interactions between cyanobacterial clock proteins KaiA and KaiC. *Biochem Biophys Res Commun* 316:195–202.

[134] Ma L, Ranganathan R (2012) Quantifying the rhythm of KaiB-C interaction for in vitro cyanobacterial circadian clock. *PLoS One* 7:e42581.

[135] Boltzmann L (1872) Weitere Studien über das Wärmegleichgewicht unter Gasmolekülen. *Sitzungsberichte Akad Wiss* 66:275–370.

[136] Murayama Y, et al. (2011) Tracking and visualizing the circadian ticking of the cyanobacterial clock protein KaiC in solution. *EMBO J* 30:68–78.

[137] Villarreal Sa, et al. (2013) CryoEM and molecular dynamics of the circadian KaiB-KaiC complex indicates that KaiB monomers interact with KaiC and block ATP binding clefts. *J Mol Biol* 425:3311–3324.

[138] van Kampen NG (2007) *Stochastic Processes in Physics and Chemistry* (Elsevier, North-Holland), Third edition, p 463.

[139] Battle C, et al. (2016) Broken detailed balance at mesoscopic scales in active biological systems. *Science* 352:604–607.

[140] Oyama K, Azai C, Nakamura K, Tanaka S, Terauchi K (2016) Conversion between two conformational states of KaiC is induced by ATP hydrolysis as a trigger for cyanobacterial circadian oscillation. *Sci Rep* 6:1–11.

[141] Abe J, et al. (2015) Atomic-scale origins of slowness in the cyanobacterial circadian clock. *Science* 349:312–316.

[142] Viani MB, et al. (2000) Probing protein-protein interactions in real time. *Nat Struct Biol* 7:644–647.

[143] Gillespie DT (1977) Exact stochastic simulation of coupled chemical reactions. *J Phys Chem* 81:2340–2361.

[144] Gillespie DT (2007) Stochastic simulation of chemical kinetics. *Annu Rev Phys Chem* 58:35–55.

[145] Winfree AT (1980) *The geometry of Biological Time* (Springer, New-York), 2nd edition.

[146] Ouyang Y, Andersson CR, Kondo T, Golden SS, Johnson CH (1998) Resonating circadian clocks enhance fitness in cyanobacteria. *Proc Natl Acad Sci* 95:8660–4.

[147] Woelfle MA, Ouyang Y, Phanvijhitsiri K, Johnson CH (2004) The adaptive value of circadian clocks: An experimental assessment in cyanobacteria. *Curr Biol* 14:1481–1486.

[148] Hatakeyama TS, Kaneko K (2012) Generic temperature compensation of biological clocks by autonomous regulation of catalyst concentration. *Proc Natl Acad Sci* 109:8109–8114.

[149] Hatakeyama TS, Kaneko K (2015) Reciprocity between robustness of period and plasticity of phase in biological clocks. *Phys Rev Lett* 115:1–5.

[150] Hasegawa Y, Arita M (2014) Optimal implementations for reliable circadian clocks. *Phys Rev Lett* 113:1–5.

[151] Kidd PB, Young MW, Siggia ED (2015) Temperature compensation and temperature sensation in the circadian clock. *Proc Natl Acad Sci* 112:E6284–E6292.

[152] Schmitz O, Katayama M, Williams SB, Kondo T, Golden SS (2000) CikA, a bacteriophytochrome that resets the cyanobacterial circadian clock. *Science* 289:765–768.

[153] Hosokawa N, Kushige H, Iwasaki H (2013) Attenuation of the posttranslational oscillator via transcription-translation feedback enhances circadian-phase shifts in Synechococcus. *Proc Natl Acad Sci* 110:14486–14491.

[154] Wood TL, et al. (2010) The KaiA protein of the cyanobacterial circadian oscillator is modulated by a redox-active cofactor. *Proc Natl Acad Sci* 107:5804–5809.

[155] Kim YI, Vinyard DJ, Ananyev GM, Dismukes GC, Golden SS (2012) Oxidized quinones signal onset of darkness directly to the cyanobacterial circadian oscillator. *Proc Natl Acad Sci* 109:17765–17769.

[156] Yoshida T, Murayama Y, Ito H, Kageyama H, Kondo T (2009) Nonparametric entrainment of the in vitro circadian phosphorylation rhythm of cyanobacterial KaiC by temperature cycle. *Proc Natl Acad Sci* 106:1648–1653.

[157] Pattanayak GK, Phong C, Rust MJ (2014) Rhythms in energy storage control the ability of the cyanobacterial circadian clock to reset. *Curr Biol* 24:1934–1938.